Solid-State Electronics Pergamon Press 1962. Vol. 5, pp. 11–37. Printed in Great Britain

ACCURATE SOLUTION OF AN IDEALIZED ONE-CARRIER METAL-SEMICONDUCTOR JUNCTION PROBLEM*

J. ROSS MACDONALD

Texas Instruments Incorporated, Dallas 22, Texas

(*Received* 26 *June* 1961; *in revised form* 25 *September* 1961)

Abstract—An accurate digital-computer solution is presented of the differential equations describing an idealized metal-semiconductor junction. Mobile charges of negative sign only are considered which arise from a uniform, fixed-donor charge distribution. The situation is similar to that considered earlier by WAGNER, SCHOTTKY and SPENKE, and accurate results for the static current–voltage characteristic and distance dependence of field, electrostatic potential, and quasi-Fermi-level potential are compared with previous approximate results. Primary attention is devoted to a structure involving one ohmic and one barrier electrode separated by a fixed distance, but that involving two barrier electrodes a fixed distance apart is also investigated. The problem is idealized by omitting trapping, image effects, tunneling, recombination, breakdown and hot-electron effects. Earlier approximate treatments are rather inaccurate in their predictions of the space dependence of various quantities but are quite close in their current-voltage predictions, even in the forward-bias direction of current flow. The results for a fixed length of material between electrodes are compared with those of the more usual approximate analyses which pertain to a variable-length barrier region alone. The influence of the fixed length, which corresponds to the experimental situation, is large, under some conditions, on current–voltage relations, resistance and on the forward and reverse differential capacitance of the system.

Résumé—Une solution exacte applicable aux calculatrices électroniques des équations différentielles qui décrivent une jonction idéalisée métal-semiconducteur est présentée. Des charges mobiles ayant un signe négatif ne sont considérées que lorsqu'elles proviennent d'une distribution de donneur uniforme et fixe. Le cas est similaire à celui analysé précédemment par WAGNER, SCHOTTKY et SPENKE; des résultats exacts décrivant la caractéristique statique courant-tension, la dépendance du champ en fonction de la distance, le potentiel électrostatique, et le potentiel des niveaux quasi-Fermi sont comparés avec de précédents résultats approximatifs. Une attention particulière est consacrée à une structure comprenant une électrode ohmique et une autre de barrière séparée par une distance fixe, mais on a aussi considéré une autre structure comprenant deux électrodes de barrière séparées par une distance fixe. Le problème est idéalisé en omettant les effets de trappe, d'image, de tunnel, de recombinaison, de disruption, et d'electrons "chauds". Precédemment les traitements approximatifs étaient plutôt inexacts en ce qui concenrait les prédictions de la dépendance de charge de plusieurs quantités mais étaient plus justes en ce qui concernait les prédictions courant-tension, même dans le sens avant de l'écoulement du courant. Les résultats ayant rapport à une longueur fixe de matériau entre électrodes sont comparés avec ceux des analyses approximatives plus usitées qui ont rapport à une seule région de barrière à longueur variable. L'influence de la longueur fixe, qui correspond au cas expérimental, est importante sous certaines conditions sur les relations courant-tension, résistance et sur la capacité différentielle en sens avant et inverse du système.

Zusammenfassung—Für die Differentialgleichung eines idealen Metall-Halbleiter-Übergangs wird eine genaue Digitalrechner-Lösung gegeben. Die Behandlung beschränkt sich auf bewegliche Ladungen negativen Vorzeichens, die durch eine gleichförmige, bestimmte Verteilung der Donatorladung entstehen. Dies entspricht den früher von WAGNER, SCHOTTKY und SPENKE behandelten Bedingungen, und die genauen Ergebnisse für die statische Strom-Spannungs-Kennlinie und die Abhängigkeit des Feldes, elektrostatischen Potentials und des quasi-Fermi-Niveau Potentials vom Abstand werden mit den früheren angenäherten Ergebnissen verglichen. In

* Many of the present results were presented at the Houston, Texas, meeting of the American Physical Society, 5 March 1960.

erster Linie wird ein Gebilde behandelt, das eine ohmsche und eine Sperrelektrode mit festem Abstand enthält, daneben wird auch der Fall von zwei Sperrelektroden mit festem Abstand in Betracht gezogen. Durch Vernäehlässigung von Einfang, Bildwirkung, Tunneleffekt und der Wirkung von Rekombination, Durchschlag und heissen Elektronen wird das Problem idealisiert. Die früheren Näherungsverfahren sind in Bezug auf Angaben über die räumliche Abhängigkeit der verschiedenen Grössen etwas ungenau, dagegen sind die Angaben uber die Strom-Spannungs-Beziehung, sogar im Falle einer Vorspannung in der Flussrichtung, ziemlich genau. Ergebnisse für eine bestimmte Materiallänge zwischen den Elektroden werden mit den ublichen Annäherungslösungen, die sich auf eine veränderliche Sperrschichtlänge beziehen, verglichen. Die festliegende Länge, die den Versuchsbedingungen entspricht, übt unter gewissen Verhältnissen einen starken Einfluss auf Strom-Spannungs-Beziehungen, Widerstand und die differentielle Kapazität des Systems in Fluss- und Sperrrichtung aus.

INTRODUCTION

THE charge distribution in a vacuum or a material medium is determined by the boundary conditions and by constraints within the medium. Table 1 presents a non-exhaustive classification of some cases of usual interest based on the above distinctions. An idealized physical situation can be approximated by the combination of one choice from the left-hand column with one from the right-hand; thus, the case I,A might pertain to electrons in a vacuum or solid with boundary electrode(s) which are blocking for electrons. Although mobile charges of a given sign which are present may be of different types and have different mobilities, in the usual case considered theoretically the situation is simplified and all mobile charges of the same sign are taken to have the same mobility. This restriction, plus that of one-dimensionality, will be adhered to herein. Note that zero recombination of mobile carriers is equivalent to complete ionization of any neutral centers from which they arise. It is well approximated in weak electrolytes and is the limiting high-temperature condition in extrinsic semiconductors.

Although the present work will be largely devoted to case II(1),B(a), some discussion of the historical development of solutions to other cases as well is in order. Attention seems first to have been devoted to case I,C(1,a) in connection with diffuse double layers in electrolytes.[1,2] The solution of the potential distribution in the diffuse layer for a single, plane, blocking electrode was first given by GOUY[1] and in modern form by FOWLER[3] but has sometimes been attributed to MÜLLER[4]. It has been re-derived independently many times thereafter, especially since the advent of the transistor.[5,6] The expressions for the static and differential capacitances of the simple diffuse double layer have been given by

Table 1. *Classification of cases*

Current conditions	Internal conditions
I. Zero current; thermal equilibrium	A. Mobile charges of only one sign present
II. Non-zero current; steady state	B. Mobile charges of one sign plus fixed recombination centers present
1. d.c.	a. Zero recombination
2. a.c.	b. Non-zero recombination
III. Transients	C. Mobile carriers of both signs present
1. Charging	1. Intrinsic or injected charge
a. Zero final current	a. Zero recombination
b. Non-zero final current	b. Non-zero recombination
2. Discharging	2. Extrinsic
a. One or both electrodes blocking	a. Zero recombination
b. Electrodes not or partly blocking	b. Non-zero recombination

GRAHAME[7] and by the author[8] and have recently been presented again by BOHNENKAMP and ENGELL[9].

A detailed discussion of potential distributions and capacitance in cases I,B(a) and I,B(b) for both one[10] and two[11] blocking electrodes has recently been given by the author. A somewhat similar treatment of solely potential distributions has been published by PROCTOR and SUTTON[12], but it is incorrect in some of its conclusions. The differential capacitance for a single blocking electrode in case I,B(a) was apparently first calculated by WAGNER[13], although this fact seems to be little recognized today. BOHNENKAMP and ENGELL[9] have given an expression for the capacitance for case I,C(2,a) which reduces to WAGNER's result when intrinsic carriers are ignored. Recently, DEWALD[14] has recalculated the capacitance for a single blocking electrode in cases I,B(a) and I,B(b) and applied the results to zinc oxide.

Since the advent of the transistor, considerable progress has been made in the small-signal treatment of transient and a.c. response problems involving mobile charge. On other hand, little progress has been achieved in the exact large-signal solution of these problems, and they will not be considered further herein. Instead, further discussion will be restricted to the direct-current case only.

The early theories of rectification between a metal and a semiconductor are well discussed by HENISCH[15] and by SPENKE[16]. We shall here be primarily concerned only with barrier-layer rectification theories which correspond to cases II(1),A or II(1),B(a). In the latter case, any minority carriers present will be neglected, and immobile impurity centers will be assumed uniformly distributed throughout the semiconductor. This is the situation which leads to the ideal Schottky barrier[17].

The first exact solution of case II(1),A for specified boundary charge concentrations was that of FAN[18a], who applied his results, expressed in terms of Airy integrals, to copper oxide rectifiers.* FAN also gives a solution for case I,A. FAN's basic differential equation was rederived later by SHOCKLEY and PRIM[19a] and solved exactly with different boundary conditions to apply to the case of space-charge-limited emission in a *p–i–p* structure.† Here results were expressed in terms of modified Bessel functions of fractional order. Neglecting diffusion effects, DACEY[20] gave a treatment of the same problem with a field-dependent mobility. Next, without reference to the work of FAN[18a] and of SHOCKLEY and PRIM[19a], SKINNER[21,22] published solutions for cases I,A and II(1),A which are appropriate for describing the charge conditions in some insulators. For non-zero current, SKINNER's results are expressed in terms of ordinary and modified Bessel functions of fractional order.

In all the above solutions, trapping effects have been neglected. SUITS[23] has extended SKINNER'S results for case II(1),A to include trapping of mobile charge by originally uncharged centers. Although the treatment of trapping is approximate and only valid when the trap occupancy is low, an analytic solution in terms of Bessel functions of fractional order is obtained which applies when the charge densities at the boundaries of a slab of insulator are held fixed and independent of current through it. Earlier, LAMPERT[24] gave an approximate treatment (in which diffusion effects were neglected), of space-charge-limited currents in insulators with traps and later[25] extended these results to the case of field-dependent mobility. It should be pointed out that in those cases where field-dependent mobility is considered, such as the treatments of DACEY[20] and of LAMPERT[24,25], the mobility and diffusion constant should depend on current as well as field in such a way as to give no field dependence in the zero-current thermal-equilibrium case obtained, for example, with a blocking electrode.

Very little work has been done on the two-carrier, non-zero-current, space-charge problem because of its difficulty. Recently, however

* FAN's solution is apparently not well known. For example, a solution of the equations in terms of Bessel functions has recently been republished independently by ADIROVICH[18b]. In addition, it was not referred to in a recently published treatment of space-charge-limited currents by WRIGHT[18c]. Solutions for the zero-current case I,A have been known for a long time and are cited by SKINNER (see Ref. 21, below).

† The fact that FAN's results can be expressed in terms of Bessel functions of fractional order has not usually been recognized but was apparently first pointed out by LANDSBERG[19b].

PARMENTER and RUPPEL[26] have treated case II(1),C(1,b) for injected charge of both signs. The insulator has been assumed trap-free and diffusion has been neglected. LAMPERT[27] has given a further simplified treatment of this problem, including consideration of recombination mechanisms and field-dependent carrier mobilities. Recently, LAMPERT[28] has also extended the simplified solution which neglects diffusion to the semiconductor case with injection II(1),C(2,b). The neglect of diffusion necessitates the rather artificial boundary conditions that the field be zero at both anode and cathode and consequently restricts the range of applicability of solutions of this type.

In most space-charge work, it has been customary to use the Maxwell–Boltzmann distribution for mobile carriers in the thermal-equilibrium case. This simplifying restriction has been relaxed by VAN OSTENBURG and MONTGOMERY[29] for charge of a single-sign mobile and by SEIWATZ and GREEN[30] for the more general semiconductor case. In addition, DEWALD[14] has given an approximate treatment of the capacitance arising in case I,B for degenerate conditions. These are all equilibrium calculations, however, and no potential distributions or current–voltage results are obtained. The results obtained apply for very heavy doping and/or low temperatures.

MOLL[31] has summarized the historical development of the theory of the current–voltage relation for *p–n* junctions II(1),C(2,b), and it therefore need not be repeated here. We shall concentrate attention primarily on case II(1),B hereafter. This case applies to a metal–semiconductor contact in which minority carriers are neglected either because of heavy extrinsic doping of the semiconductor or because of a low relative temperature of operation. It also is pertinent to the situation where the metal is replaced by a concentrated electrolyte. It applies as well to an insulator with metal or other partly blocking contacts where the mobile carriers of one sign are dissociated from neutral centers by the absorption of radiation. Finally, this case is also pertinent to the metal–metal oxide-electrolyte situation, which also exhibits rectification[32] and is of considerable practical importance.

Fig. 1 shows very diagrammatically some of the charge arrangements which can arise in case

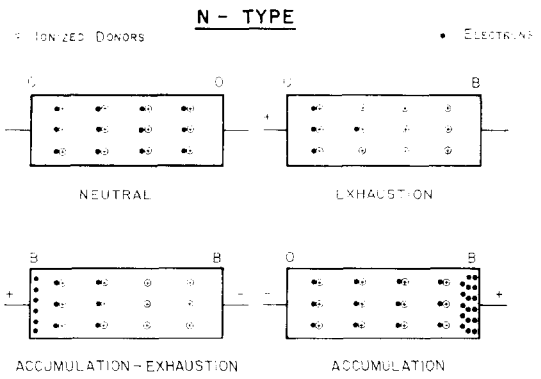

FIG. 1. Diagrammatic representation of space-charge with ohmic [O] and blocking [B] electrodes.

I,B(a) with ohmic (O) and completely blocking (B) contacts. In the neutral case, there are no macroscopic potential drops within the system, and conduction-band electrons remain close to ionized donors. With one blocking and one ohmic contact, mobile carriers are free to leave or enter the material under the influence of an externally applied potential or potential barrier at the blocking electrode. Exhaustion or accumulation regions may be formed under these circumstances as shown. When both contacts are blocking, both regions appear but are restricted in magnitude by conservation of charge within the material as a whole[10,11]. Such blocking conditions may be well approximated by interposing a thin insulating layer between the metallic electrodes and the charge-containing material or by placing the material without electrodes in a region of high electric field such as that produced in semiconductor field-effect experiments. In the present work, we shall usually make no distinction between exhaustion and depletion but shall use the word "exhaustion" to include the depletion, or incomplete exhaustion, case as well.

In case II(1),B(a), the situation may be expected to remain qualitatively similar, for very small currents, to that discussed above. For a current to flow without tunneling or barrier breakdown, it is necessary that both contacts be ohmic or only partly blocking. Instead of the infinitely high potential barrier of an ideal blocking electrode, the potential barriers at the electrodes must be finite in height. When a reverse potential is applied

to a system having one ohmic and one partly blocking electrode, the effective height of the barrier will be increased, while a forward potential will decrease the height until finally the barrier disappears and essentially ohmic conduction is reached at high forward currents.

In barrier-layer devices, rectification is associated with a layer next to a partly blocking contact which is partly depleted or completely exhausted of mobile charge carriers. When this layer is thick compared to the mean-free-path length of mobile carriers, the diffusion theory of rectification applies, while in the opposite extreme of thin barrier layers, the diode theory is appropriate.[15] In the present work we shall treat only the usual case of complete ionization (zero recombination) and thick barriers. Although the assumption of complete ionization is only a limiting case for solids and occurs only at infinite temperatures or radiation intensities, many practical situations arise where this assumption is a good approximation. In later work it is hoped to investigate in some detail the case of rectification with non-zero recombination.

Two different assumptions have been made in the diffusion theory of rectification concerning the barrier-layer thickness. For the MOTT[33] barrier it is assumed that the concentration of donors is vanishingly small for a certain distance from the partly blocking metal electrode into the material of the rectifier, and that there is then an abrupt transition to a high donor concentration. For such barrier layers of constant thickness, the electric field in the barrier is also constant. On the other hand, for the Schottky barrier it is assumed that the original concentration of unionized donors is uniform throughout the material, leading to a dependence of barrier layer thickness on applied potential. The assumption of a homogeneous donor distribution is more often a better approximation to the experimental rectifier situation than is the MOTT assumption, but the usual neglect of mobile charge in the barrier region, which leads to linear field dependence, is an approximation which is not always well justified, especially in the forward-bias direction. This approximation and that of somewhat arbitrarily separating out a barrier region of specific thickness (the region where the field is non-zero) is avoided in the present work, allowing the effect of the above approximations to be evaluated. Therefore, we shall usually consider a piece of material of fixed length between an ohmic and a partly blocking electrode. This configuration corresponds to that used in experimental measurements of rectifier characteristics, and its treatment will make clear how an ohmic potential drop and the geometric capacitance between the electrodes may be properly accounted for.

The simplest isothermal diffusion-theory rectification characteristic was first derived by WAGNER[13]. Soon after this, SCHOTTKY[34], SCHOTTKY and SPENKE[35], and SPENKE[36] improved the theory further, but so far no exact solution of the basic equations of the problem has been given. LANDSBERG[37] has carried out an approximate treatment with the inclusion of image force effects acting on mobile carriers near the partly blocking metal electrode. In addition, LANDSBERG has also considered the case of field-dependent mobility and diffusion constant[38] and the effect of an arbitrary distribution of fixed charge[39].

In the present work, we shall omit consideration of the following: trapping; image effects[37,40]; tunneling; recombination; non-uniform fixed charge distributions; discrete charge effects; field-dependent mobility, diffusion constant and dielectric constant; avalanche breakdown; field emission; degeneracy; and non-isothermal conditions. Although a formal non-isothermal diffusion theory of rectification is available,[41] the complexity arising from a non-isothermal lattice can be avoided by pulse measurements[42]. The work to be described here is, therefore, an accurate treatment of the popular WAGNER–SCHOTTKY–SPENKE idealized situation. This approach has been applied to the interpretation of so many different experiments that no summary of experimental applications will be given here. The present results will allow the accuracy of the simplifying assumptions made by the above authors to be assessed and should yield a basis of comparison with, later, more-sophisticated rectifier calculations. In the next section, the pertinent equations for case II(1),B(a) are set up and exact and approximate integrations leading to field, current and capacitance relations are discussed. Finally, the results of accurate computer solutions of the differential equations of the problem are considered in some detail.

NOTATION

C_0	$\epsilon/4\pi L_D$, limiting space-charge capacitance.
C_d	differential capacitance
D_n	electron diffusion constant
e	magnitude of electron charge
$\mathscr{E}$	electric field
E	$\mathscr{E}/[kT/eL_e]$, normalized electric field (number subscripts as defined in text)
E_i	energy (letter subscripts as defined in text)
j	current (subscripts as defined in text)
J	$j/[D_n e n_\infty/L_e]$, normalised current (subscripts as defined in text)
k	Boltzmann's constant
k_l	rate constants
l	electrode separation
l_m	length of mean free path
L	l/L_e, normalized length
L'	normalized length of barrier region alone in approximate theories
L_D	$[\epsilon kT/4\pi e^2 N_D]^{1/2}$, Debye length
L_e	θL_D, effective Debye length with recombination
n	negative mobile charge concentration
n_∞	value of n in space-charge-free-bulk region
N	n/n_∞, normalized negative mobile charge concentration
N_j^i	density of states; density of charge (subscripts as defined in text)
q_2	charge on barrier electrode
r	$N_{D\infty}^n/N_D$, recombination constant
$\mathscr{R}$	normalized resistance (subscripts as defined in text)
R	$k_2 N_D/k_1$, recombination constant
t	time
T	absolute temperature
V	fixed potential difference (subscripts as defined in text)
x	distance variable
X	x/L_D or x/L_e, normalized distance variable
Y	$L-X$
ϵ	E_1-J; also used for dielectric constant
η	$\ln N = \Psi-\Phi_n$
θ	$[(1+r)(1-r)]^{-1/2}$
μ_n	electron mobility
ϕ_n	$(E_{F\infty}-E_F)/e$, quasi-Fermi-level potential
Φ_n	$\phi_n/(kT/e)$
Φ_{n_2}	total normalized potential difference across sample, equal to V_a
Φ'_{n_2}	normalized quasi-Fermi-level potential difference across barrier region alone
ψ	electrostatic potential
Ψ	$\psi/[kT/e]$ (subscripts as defined in text)

FORMAL RESULTS FOR ZERO RECOMBINATION

Basic equations

The equations describing the steady-state behavior of an n-type semiconductor in which intrinsic carriers are neglected are, for one-dimensional variation,

$$\frac{d\psi}{dx} = -\mathscr{E} \tag{1}$$

$$\frac{d\mathscr{E}}{dx} = \frac{4\pi e}{\epsilon}(N_D^+ - n) \tag{2}$$

$$j = j_n = eDn\left[(en\mathscr{E}/kT) + \frac{dn}{dx}\right] \tag{3}$$

$$\frac{dj}{dx} = 0 \tag{4}$$

where the Einstein relation $\mu_n/D_n = e/kT$ has been used in (3). In these equations, e is the magnitude of the electron charge and ϵ the dielectric constant of the material. The other symbols have their conventional meanings. In the present zero-recombination case, the donors are completely dissociated and $N_D^+ = N_D$, the original, spatially uniform donor concentration. A short treatment of the equations pertinent in the non-zero-recombination case is presented in Appendix I as a background to future work in this field. When the material is degenerate, the charge densities in (2) obey Fermi–Dirac statistics,[43] and LANDSBERG[44] has shown that the mobilities and diffusion constants are concentration dependent. In addition, in the case of hot electrons, it is likely that even the form of (3) must be modified.[45]

In bulk material in the absence of space charge, $n = N_D^+ = N_D$, and it will be convenient to denote this value of n by n_∞ and use it for normalization. The normalized mobile charge density is then $N \equiv n/n_\infty \equiv n/N_D$. We shall be concerned here only with temperature and doping conditions for which Maxwell–Boltzmann statistics will be a good approximation for the mobile electrons.[46,47] This requires that the concentration of conduction-band electrons always be much less than the effective density of states in the conduction band, N_c. Denote the quasi-Fermi, donor and bottom of the conduction band levels by E_F, E_D and E_C, respectively. Further, let the thermal-equilibrium, space-charge-free bulk values of these quantities be designated by the subscript ∞. Then n may be written,[47]

$$n = N_c \exp[(E_F - E_C)/kT] \quad (n \ll N_c) \tag{5}$$

Under steady-state non-equilibrium conditions, the Fermi band energy will vary with position

within the material, and it will prove convenient to describe such variation with a quasi-Fermi-level potential.[48] Let us define

$$\phi_n \equiv -(E_F - E_{F_\infty})/e \tag{6}$$

$$\psi \equiv -(E_C - E_{C_\infty})/e \tag{7}$$

where ψ is the electrostatic potential and ϕ_n is a quasi-Fermi-level potential for electrons, both taken as zero in space-charge-free bulk material. The true quasi-Fermi-level potential is simply $-E_F/e$. From (5) we may write

$$n/n_\infty \equiv N = \exp[\{(E_F - E_{F_\infty}) - (E_C - E_{C_\infty})\}/kT]$$
$$= \exp[e(\psi - \phi_n)/kT] \equiv \exp[\Psi - \Phi_n] \tag{8}$$

where Ψ and Φ_n are normalized quantities. Their difference $(\Psi - \Phi_n)$ will be denoted by ηx.

In addition to the above normalization, it will prove convenient to introduce $E \equiv eL_D\mathscr{E}/kT$, $X \equiv x/L_D$, $L \equiv l/L_D$, $Y \equiv L - X$, and $J \equiv L_D j_n/eD_n n_\infty$. Here l is the length of a slab of material between two plane, parallel electrodes, an essentially ohmic one at $x = 0$ and a partly blocking one at $x = l$. L_D is the Debye length for zero recombination, $L_D \equiv (\epsilon kT/4\pi e^2 N_D)^{1/2}$. With these definitions the pertinent normalized equations become

$$\frac{d\Psi}{dX} = -E \tag{9}$$

$$\frac{dE}{dX} = 1 - N = 1 - \exp(\Psi - \Phi_n) \tag{10}$$

$$\frac{d\Phi_n}{dX} = -J \exp(\Phi_n - \Psi) \tag{11}$$

This set of equations can be reduced to two differential equations involving E and η only, but, since it is important to be able to separate out the variations of Ψ and Φ_n individually, their equations have been kept separate. When there is no fixed space charge,[18,19] (10) becomes $dE/dX = -N$ and the other equations remain unchanged.

Fig. 2 shows energy-band diagrams for a metal–semiconductor junction, expressed in terms of the present variables, for three current conditions. The current directions shown represent conventional current; electrons will travel in the opposite direction. It will be noted that for convenience the flat band condition has been taken at the extreme left of each diagram. The normalized diffusion voltage V_D shown is the height of the barrier in the equilibrium case and is positive for an exhaustion–depletion barrier region such as that shown in Fig. 2. It may be

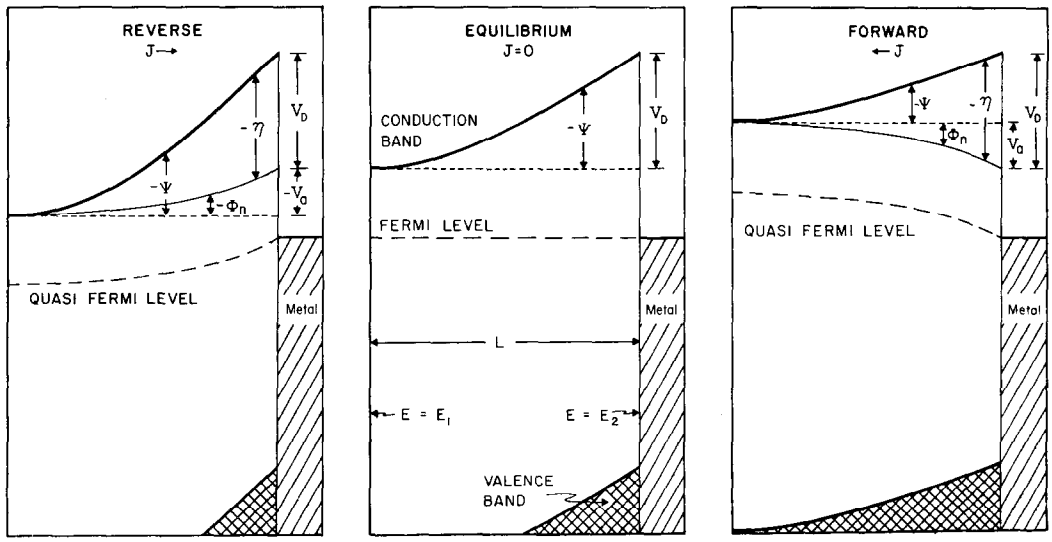

FIG. 2. Energy-band diagrams for semiconductor-metal junction.

related to the properties of the metal and semiconductor in various ways which are discussed in detail by SPENKE[49]. If we use a subscript 2 to denote the value of a quantity at the barrier, it is clear that $V_D = -\eta_2 = (\Phi_{n_2} - \Psi_2)$ in the present case. Further, the normalized applied voltage V_a equals Φ_{n_2}. Since Φ_{n_1} is here zero, this result is in agreement with the rule that the voltage applied across a region equals the difference in quasi-Fermi-level potentials at the ends.

As mentioned earlier, the equations of the diffusion theory of rectification are appropriate when the mean free path of current carriers is small compared to the barrier-region thickness. material which is not too heavily doped and is non-degenerate. For an exhaustion situation, the magnitude of E increases with reverse bias; therefore, the first condition limits the bias range over which the present equations are applicable. The second condition is usually less restrictive but, when combined with equation (10), limits the range of applicability of the equations in a charge accumulation situation where N may be much greater than unity.

For convenience hereafter, we shall often use the same word to designate both a normalized and an unnormalized quantity, since the specific meaning will be evident from the symbols em-

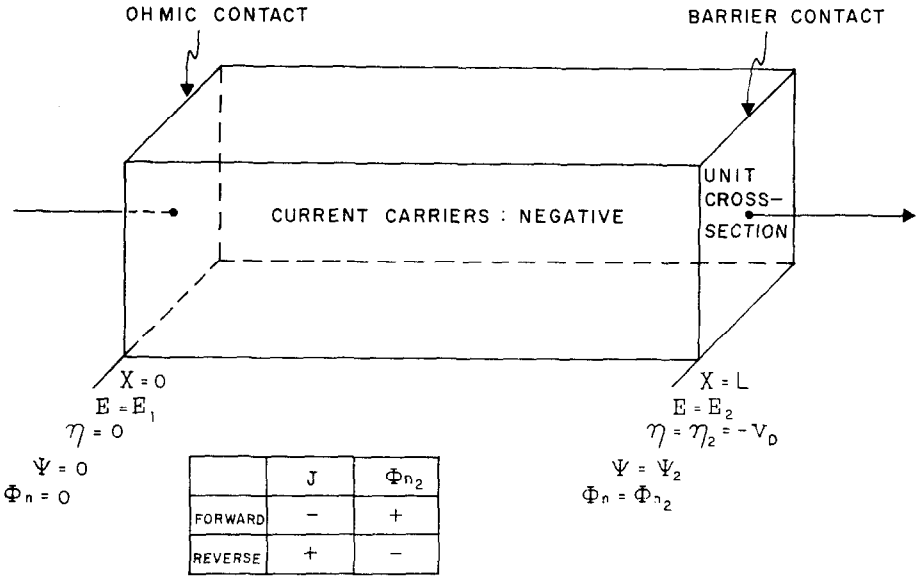

FIG. 3. Structure analysed and boundary conditions.

STRATTON[50] has obtained more precise requirements by deriving the diffusion equation from the Boltzmann transport equation. The conditions simplify considerably in the present idealized case where the current carriers are taken to have very nearly the lattice temperature. If $L_m \equiv l_m/L_e$, where l_m is the mean-free-path length for the mobile carriers, the requirements are, firstly, the usual condition $|E|L_m \ll 1$ and, in addition, $L_m^2|dE/dx| \ll 1$. The mean free path will be of the order of 10–10^3 Å for most materials of interest, and L_m will thus be appreciably less than unity for ployed. In addition, we shall focus attention on a cross-section of material of unit area and will therefore omit verbal distinction between such quantities as currents and current densities, capacitance and capacitance per unit area, etc.

Exact and approximate results

The situation with which we shall usually be concerned is depicted in Fig. 3. For the boundary conditions at the ohmic contact we have somewhat arbitrarily chosen a zero space-charge condition such as that shown at the left of each section of

Fig. 2. Although there may be a small electric field, E_1, at this point, the free electron concentration at the contact is constrained, if necessary by a special electrode, to equal n_∞, which, in the present zero-recombination case, is itself equal to N_D. variation is entirely specified by the magnitudes and signs of E_1 and J, allowing the construction of Fig. 4 which divides the J–E plane into six regions and one singular line as shown. This figure applies only for integration in the $+X$-

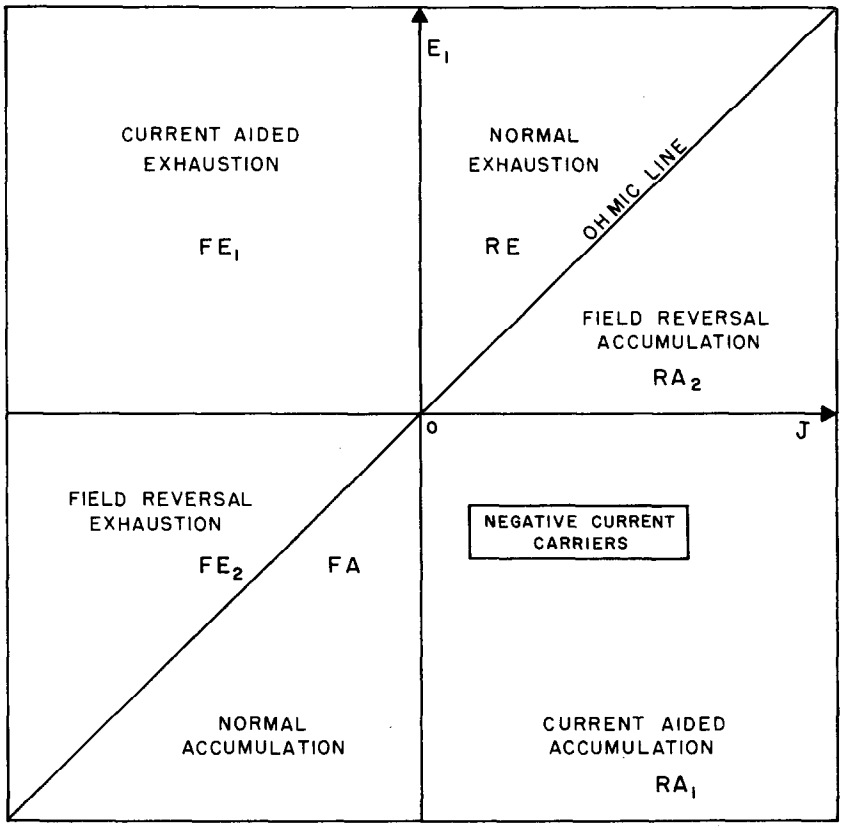

FIG. 4. Diagram showing influence of E_1 and J on character of space charge for integration in the $+X$ direction from an ohmic contact.

Alternatively, E_1 could have been taken identically zero and some space charge accepted at the "ohmic" electrode. The present choice is simplest for the following reasons: only one quantity need be specified at this boundary instead of two; it is experimentally realizable; it allows Ψ_1 and Φ_{n_1} to be always taken as zero; and it is not particularly restrictive of the complexity of solutions possible for the system.

It is possible to infer qualitatively from the forms of equations (9–11) how the space charge will vary as one progresses from left to right. This direction. The letters F, R, A and E stand for forward, reverse, accumulation and exhaustion, respectively. When $E_1 = J$, no space-charge region is formed, no matter how much X increases, and the material remains completely ohmic. For all other cases, one of the conditions shown on Fig. 4 applies as the equations are integrated in the direction of positive X away from the ohmic electrode. In the present work, we shall primarily be interested in the exhaustion regions to the left of the ohmic line, since only they exhibit sufficient rectification to be of technical interest. Fig. 4

shows that there are three distinct exhaustion regions. The closer E_1 is to J or, equivalently, the smaller the parameter $\epsilon \equiv E_1 - J$, the larger L will be for a given V_D. For a given J and E_1, L will be greatest for the FE_2 region and smallest for the FE_1 region, with the result for the RE position intermediate.

It is important to note that a single exact integration of (10) is possible in the present zero-recombination case[45] even for non-zero current. On using (9) and (10), we have

$$-E\frac{dE}{d\Psi} = 1 - \exp(\Psi - \Phi_n) \tag{12}$$

$$-\tfrac{1}{2}[E^2 - E_1^2] = \int_0^{\Psi} [1 - \exp(\Psi - \Phi_n)]\, d\Psi$$

$$= \Psi - \int_0^{\Psi - \Phi_n} e^{\eta}\, d\eta - \int_0^{\Phi_n} \exp(\Psi - \Phi_n)\, d\Phi_n$$

$$= \Psi + 1 - \exp(\Psi - \Phi_n) + J \int_0^X dX \tag{13}$$

$$E^2 - E_1^2 = 2[\exp(\Psi - \Phi_n) - 1 - \Psi - JX] \tag{14}$$

where (11) has been used in (13). Note that if there were no fixed charge, as in case II(1),A, only the $-\Psi$ in (14) would be missing. Equation (14) is in agreement with the corresponding result in the zero-current case,[10] where $J = 0$, $\Phi_n = 0$ and where E_1 is also zero when the ohmic contact is removed to infinite distance. Equation (14) could be used to eliminate equation (10) from the equations which must be solved to obtain the X dependence of E, Ψ and Φ_n for given E_1 and J. Since an exact equation analogous to (14) cannot be obtained in the $R > 0$ case, we have preferred, however, to solve equations (9–11) together, using a digital computer and employing (14) as a checking equation on the computer results when $R = 0$. When (14) is evaluated at $X = L$, one obtains the following exact equation for the current

$$J = \frac{1}{L}[\exp(-V_D) - 1 + V_D - \Phi_{n_2} - \tfrac{1}{2}(E_2^2 - E_1^2)] \tag{15}$$

Note that we have taken $V_D \equiv -\eta_2$ and that Φ_{n_2} is the voltage applied across the material of length L.

In the usual Schottky barrier approximation, the mobile charge in the barrier region is neglected. Integration of equation (10) from the partly blocking electrode toward the ohmic electrode (using the normalized distance variable Y) then yields $E(Y) = E_2 - Y$, a linear field dependence. Since the Schottky barrier deals only with the non-ohmic space-charge region, we shall denote the normalized thickness of this layer by L' rather than the previously used L, which may exceed this thickness. Since E_1 is usually quite small, we shall here adopt the usual Schottky approximation and take it zero at $Y = L'$. The potential distribution is found, using (9) and the linear field dependence, to be $\Psi = \Psi_2 + E_2 Y - (Y^2/2)$. At $Y = L'$ the condition $E_1 = 0$ yields $E_2 = L'$. If Ψ_1 is taken as zero, the potential equation then leads to the usual result

$$E_2 = \pm \sqrt{(-2\Psi_2)} = \pm \sqrt{[2(V_D - \Phi_{n_2})]} \tag{16}$$

When E_1 is taken zero, equation (15) shows that a better approximation will be

$$E_2 = \pm [2\{V_D - \Phi_{n_2} - 1 + \exp(-V_D) - JL'\}]^{1/2} \tag{17}$$

where $\exp(-V_D)$ may usually be neglected against unity. Since the JL' term will be small over most of the range of interest, it may also usually be neglected. For exhaustion barrier layers, the plus sign in (16) and (17) must be used.

Using the above expression for the space dependence of Ψ, (11) may now be rewritten as

$$\exp(-\Phi_n)\frac{d\Phi_n}{dY} = J \exp[-\Psi_2 - E_2 Y + (Y^2/2)] \tag{18}$$

When this expression is integrated with the neglect of the Y^2 term, a relatively simple expression for $\Phi_n(Y)$ may be obtained. Taking

$\Phi_n(0) = \Phi_{n_2}$ and $\Phi_n(L') = 0$ allows the constants of integration to be evaluated and leads to the following current–voltage relationship,

$$J = E_2 \exp(-V_D)[1-\exp(\Phi_{n_2})]/[1-\exp(-E_2L')] \tag{19}$$

When L' is set equal to E_2 and E_2 specified by (16), the usual Schottky barrier result is obtained.[51] A better approximation will be produced, however, by taking E_2 from (17) with the JL' term neglected and $L' = E_2$.

Increased accuracy may be achieved by integrating (18) as it stands. The following current–voltage relation is then obtained,

$$J = \frac{\exp(-V_D)[1-\exp(\Phi_{n_2})]}{\sqrt{2}\exp\{-E_2^2/2\}[\operatorname{erfi}\{(L'-E_2)/\sqrt{2}\}+\operatorname{erfi}\{E_2/\sqrt{2}\}]} \tag{20}$$

where

$$\operatorname{erfi}(\xi) = \int_0^{\xi} \exp(x^2)\,dx$$

If L' is taken equal to E_2, the first erfi function disappears. Then E_2 can be substituted from either (16) or (17). The former choice leads to the result found by SPENKE[36]. Because of the neglect of the free-charge carriers in the barrier region, equations (19) and (20) should not be expected to hold accurately into the high forward-current region where $\Phi_{n_2} \simeq V_D$. Also, it should be remembered that they apply to the barrier of length L' alone, not to the entire length L.

The exact calculation of the differential capacitance of a finite-length device with space charge and a leaky barrier is difficult under non-zero-current conditions. Operationally, this capacitance may be obtained in the limit of low frequencies from the reactive part of the fundamental-frequency current which flows when the combination of a steady bias and an infinitesimal sinusoidal voltage is applied to the device. In the absence of an exact solution of the differential equations of the problem in this case, we shall use the following approximate expression for the differential capacitance C_d

$$C_d = \left|\frac{dq_2}{d\phi_{n_2}}\right| = \left|\frac{dq_2}{d\psi_2}\right| = C_0\left|\frac{dE_2}{d\Phi_{n_2}}\right| \tag{21}$$

where $C_0 = \epsilon/4\pi L_D$ is the space-charge capacitance of a single completely blocking barrier in the limit of zero barrier height.[10,52] Here q_2 is the charge on the barrier electrode, and it is assumed that there is space-charge neutrality at the other electrode. The equality of $d\phi_{n_2}$ and $d\psi_2$ follows from the assumed independence of V_D and applied voltage.

In the present instance, equation (21) is an excellent approximation to the true capacitance over most of the bias range provided the measuring frequency is sufficiently low that the system responds quasi-statically and transit times are therefore unimportant. It can, in fact, be shown[45] that equation (21) yields an upper limit when there is a retarding barrier. Further, it leads properly to the geometrical capacitance in the limit of high forward currents and is exact at zero current. Therefore, this equation will be used in the computer calculation of capacitance presented later.

The substitution of (15) in (21) yields

$$\frac{C_d}{C_0} = \left|\frac{1+L\dfrac{dJ}{d\Psi_2}-E_1\dfrac{dE_1}{d\Psi_2}}{E_2}\right| \tag{22}$$

We shall now consider the simplification of (22) in various cases. For appreciable reverse voltage, the term $E_1dE_1/d\Psi_2$ can be neglected compared to unity and the other derivative provided L is sufficiently large that the length of the exhaustion region produced by the barrier and applied reverse voltage does not begin to approach L. In the current and reverse-bias ranges of practical interest, the capacitance will then be that of the barrier region alone and we may set $L \cong L' \cong E_2$. The quantity $LdJ/d\Psi_2$ may now be evaluated from (19), yielding $-\exp(-V_D)$ when only important terms are kept. Thus C_d becomes

$$\left(\frac{C_d}{C_0}\right)_{rev} \cong \frac{1-\exp(-V_D)}{[E_1^2+2\{\exp(-V_D)-1+V_D-\Phi_{n_2}-JL]^{1/2}} \tag{23}$$

Over a wide range of reverse voltages, E_1 and JL may be neglected compared to other larger

terms. Now in the zero current case, $\Phi_{n_2} = 0$ and $V_D = -\Psi_2$. These omissions and substitutions in (23) lead to WAGNER's[13] result discussed previously. For cases of practical interest, $\exp(-V_D)$ may be neglected compared to unity. Equation (23) still differs, however, from the conventional Schottky result by the presence of the -1 term in the denominator. Its omission in the Schottky formula arises from the neglect of free charge in the barrier region and can be of some importance when comparing theory and experiment. The reverse-bias capacitance is, approximately speaking, shunted by the high barrier-region resistance, and the combination is in series with the bulk resistance.

When the entire material behaves ohmically, $V_D = 0$ and it is easy to show that $E_1 = E_2 = J = -\Psi_2/L$ and $\Phi_{n_2} = \Psi_2$. Since $dE_2/d\Psi_2 = -1/L$, one finds from (21)

$$(C_d)_{\text{ohmic}} = C_0/L = \epsilon/4\pi l \tag{24}$$

the geometric value for a material of dielectric constant ϵ between two electrodes separated by a distance l. This capacitance is, of course, shunted by the ohmic resistance between the electrodes.

In the forward-current direction, it is found that $E_1 \cong J$ very closely if L is appreciably greater than unity. Thus, C_d/C_0 becomes

$$\left(\frac{C_d}{C_0}\right)_{for} \simeq \left| \frac{1+(L-J)\dfrac{dJ}{d\Psi_2}}{E_2} \right| \tag{25}$$

where E_2 is given by (15). For sufficiently high applied forward bias, the barrier layer must eventually be wiped out even for very appreciable V_D values. Then, again, the material behaves ohmically with $E_2 \cong J \cong -\Psi_2/L$ and (25) reduces to the geometrical result L^{-1}. The same result is also found for reverse bias when the bias is so high that the exhaustion layer essentially fills the region between electrodes completely.

Next, consider the situation of one ohmic electrode and one partly blocking electrode in the limit of vanishing space charge and current: $V_D \to 0$, $\Psi_2 \to 0$, $J \to 0$. On letting J go to zero first, it is easy to show[11] that E_1 approaches $-\Psi_2/\sinh L$. Then (15) yields $E_2^2 \cong E_1^2 + \Psi_2^2 = \cong \Psi_2^2 \coth^2 L$. This result may be used in (21) to give

$$\underset{\text{Im}\,\Psi_2 \to 0}{C_d} = C_0 \coth L \tag{26}$$

in agreement with earlier results[8,10]. When $L \to \infty$ $C_d \to C_0$, the correct value for a single electrode. On the other hand, when $L \to 0$, there is no room for a space-charge layer, and C_d approaches the ohmic value given in (24).

When none of the above simplified forms is sufficiently applicable or accurate, the differential capacitance may be calculated directly from (21), with the derivatives approximated as finite differences. A possible procedure is to select L and V_D and use the digital computer to obtain results for two very nearly equal values of J. The results may then be used to determine C_d and also the differential resistance of the junction.

DISCUSSION OF COMPUTER RESULTS

Introduction

In this section, the results of extensive computer calculations for the zero-recombination case are discussed and compared with various approximate results. The outcome of similar calculations with recombination present will be reported later. Details of the computer calculations are presented in Appendix II. Since image effects have been neglected in the present treatment, the diffusion potential V_D will remain independent of current and applied voltage. This quantity, which must be positive to allow an exhaustion layer to form and which must be greater than unity for much nonlinearity to be exhibited, will generally be taken to be 10 for the present numerical work. This is a convenient magnitude and allows direct comparison with considerable earlier theoretical work where the same value has been used. The normalized length L will also usually be taken as 10, although results for many different lengths have been obtained.

Distance dependence

Fig. 5 compares some results for the field-distance dependence obtained from the SCHOTTKY and SPENKE theories already mentioned with those obtained from an accurate computer solution of the differential equations of the problem and with the approximate modified SCHOTTKY solution obtained by combining equations (17) and (19). In such combination, the JL term is omitted from

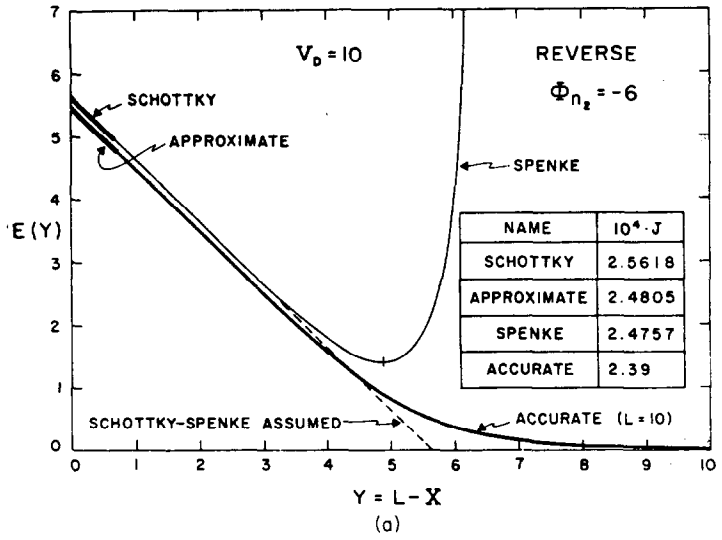

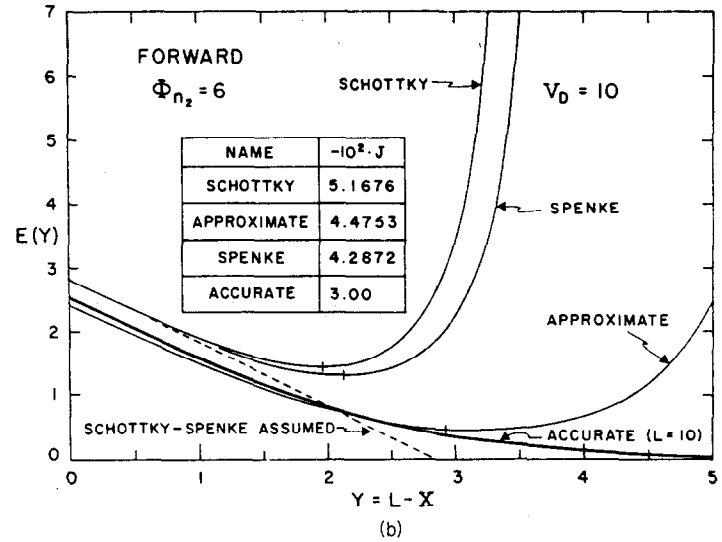

FIG. 5. Field-distance dependence for various degrees of approximation (junction at left).

(17) and L' is taken equal to E_2. The dashed lines in parts (a) and (b) of Fig. 5 show the linear field-distance dependence assumed by SCHOTTKY and SPENKE. The solid lines were obtained from computer solutions run backwards from the barrier (at $Y = 0$) toward increasing Y and using the values of J and E_2 which follow from the various approaches. Note that the same magnitude for forward and reverse bias has been used. The initial value of Ψ_2 is obtained from the bias value and V_D.

The value of J used in the machine runs are shown on the figure. For the reverse runs, the SCHOTTKY–SPENKE (S–S) values of E_2 are quite close to the accurate value, but the difference is considerably larger in the forward case. It is clear

that there is considerable discrepancy between the S–S assumed field dependence and the actual dependences obtained from accurate solution of the equations with the S–S values of J and E_2. The heavy solid lines in part (a) show the entire field dependence obtained using the SCHOTTKY and modified SCHOTTKY (termed approximate) starting conditions. After an infinitesimal initial decrease in exhaustion as integration proceeds away from the electrode, the free-charge concentration begins to drop rapidly, exhaustion reached. As integration proceeds beyond this point, an accumulation region begins to build up, Φ_n becomes limited, and Ψ and E begin to increase rapidly. When the accurate solution is run backwards, however, the condition $\Phi_n = \Psi = 0$ is reached at $Y = 10$ and the field E_1 there is 0·01462, the value selected to yield $L = 10$. If the accurate solution is continued past $Y = 10$, one again finds accumulation. The situation with both exhaustion and accumulation is shown in Fig. 6, where $\Phi_n(X)$ and $\eta(X)$ have been plotted; the

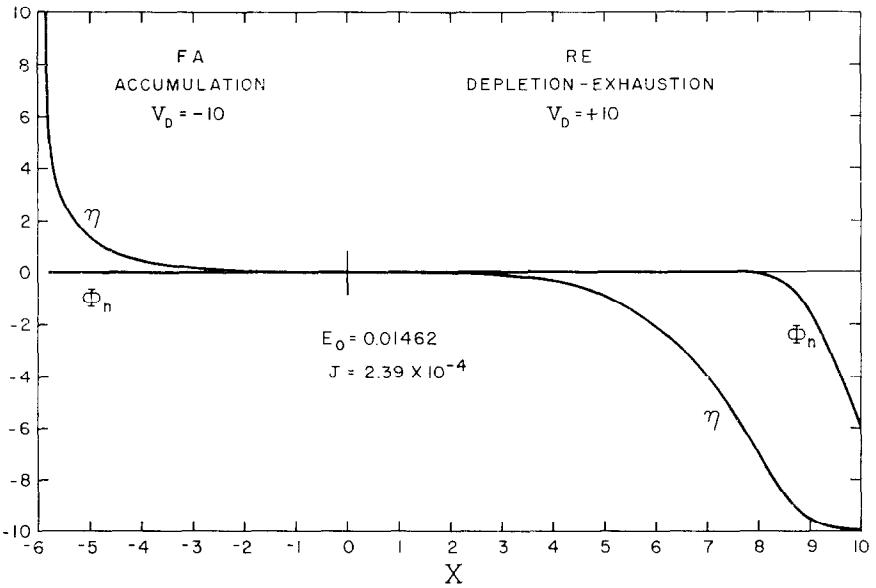

FIG. 6. Distance dependence of η and Φ_n with an accumulation junction at the left, an exhaustion junction at the right.

increases, and the solution obtained applies to a material with a larger V_D than 10. The resulting rapid increase in $\Phi_n(Y)$ precludes appreciable further increase in Y or change in Ψ and E. This increasing exhaustion behavior occurs because the initial currents in these cases are too large.

The situation is different for the reverse SPENKE case. Here, the initial current is sufficiently close to the accurate value that exhaustion only decreases. The field follows the assumed dependence quite well for a considerable distance but eventually deviates from it. At the position marked by the small vertical line, the zero space-charge condition, $N = 1$ with $\Phi_n = \Psi \neq 0$, is anode is at the left, the cathode at the right (for correspondence with the results of Ref. 11); and integration was stopped in the accumulation region when $V_D = -10$. The electrostatic potential is given by $\Phi_n(X) + \eta(X)$. Since $\ln N = \eta$, the quantity η is a logarithmic measure of the normalized charge density. The quasi-Fermi-level potential is very small over much of the region. It changes sign at $X = 0$ and reaches a maximum positive value of about 10^{-3} when $V_D = -10$.

The letters FA and RE on Fig. 6 show the regions of Fig. 4 to which the starting conditions correspond. For combined accumulation–exhaustion, the field at the zero-space-charge point

($X = 0$) has been termed E_0. Fig. 4 can be used when integration proceeds in the $-X$ direction if the labeling of the axes remains the same and the six regions denoted by letters are inverted through the origin. On the other hand, when the signs of E_1, J and X are all reversed, a complete inversion through the origin is obtained and no real change in Fig. 4 or change in the results occurs; this is readily verified from the differential equations of the problem.

Fig. 5(b) shows the assumed and actual behavior of the field in the forward current case. Here the SCHOTTKY and approximate starting conditions accumulation curves of Figs. 5(a) and 6 correspond to regions RE and FA of Fig. 4. On the other hand, the SCHOTTKY, SPENKE and modified SCHOTTKY curves of Fig. 5(b) correspond to regions FE_1 and RA_1, while the accurate curve of Fig. 5(b) and its continuation for $Y > 10$ corresponds to FE_2 and RA_2. All the results yield $E(X)$ curves which are convex to the X-axis, but those which involve FE_2 and RA_2 will be displaced downward and will cut the X-axis twice in progressing from strong accumulation to strong exhaustion. Thus, the E_0 value for the accurate solution is negative and equals $-0{\cdot}02931$ at $X = 0$.

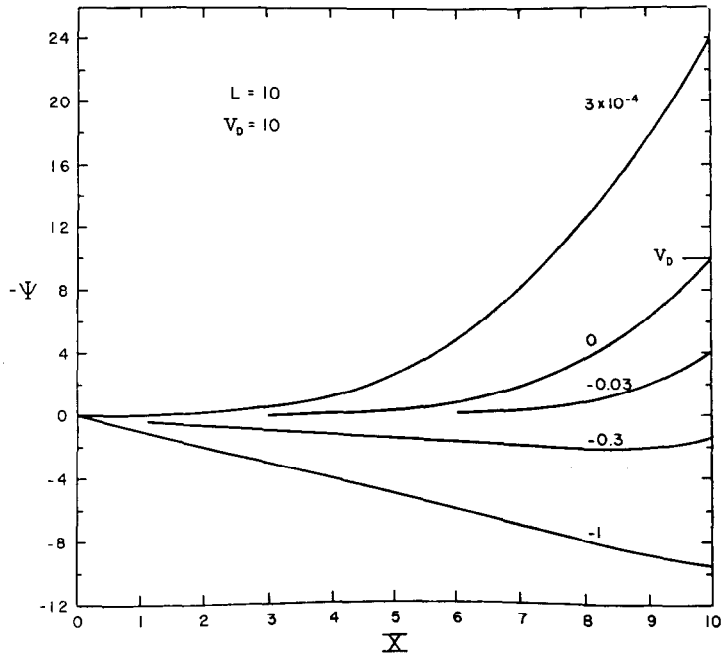

FIG. 7. Dependence of barrier profile on distance for various current values.

yield significantly better results than found in the reverse direction. The approximate solution is close to the accurate one over much of the range because its starting value of E_2 is closest to the accurate value, but deviation finally occurs because the starting current is somewhat incorrect. Again, when integration of the accurate solution is continued past $L = 10$, accumulation begins, but there are some significant differences worth pointing out. The SPENKE and accurate exhaustion–

The dependence of barrier profile on current is shown in Fig. 7. Here $-\Psi$ is plotted against X for several current values. The barrier occurs at the right for easy comparison with the qualitative curves of Fig. 2. As the forward current increases, the barrier profile is depressed until its slope, the electric field, is everywhere negative and finally approaches constancy, as in the almost ohmic $J = -1$ curve.

In Figs. 8 and 9 the distance variable Y has

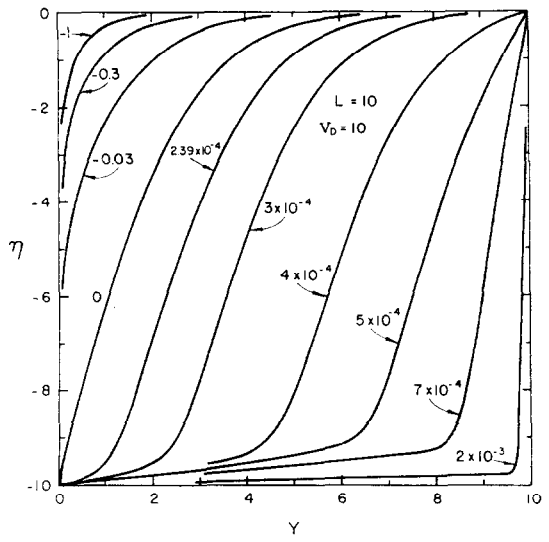

FIG. 8. Dependence of η (logarithmic charge density) on distance for various current values (junction at left).

been used in order to place the barrier contact on the left for convenient comparison with zero-current results previously obtained.[10] Fig. 8 shows η, or the logarithmic charge density, for various forward and reverse current values. The zero-current curve agrees closely with the earlier result for Ψ found by a different mathematical method. A slight difference appears for large Y values because L is taken to be 10 here and was infinite in the earlier one-blocking-electrode work.

Since the effective length of the barrier region is reduced for forward currents and increased for reverse ones, the finite length of the sample has little effect on the barrier-region charge-density distribution for forward currents, but exerts a crucial effect in the reverse direction because the exhaustion region cannot exceed the sample length. In actual physical cases, breakdown would probably occur before a distribution such as that shown for $J = 2 \times 10^{-3}$ could be set up.

Fig. 9 shows the dependence of the quasi-Fermi-level on distance for reverse and forward currents. Since the change of shape with current is of most interest, normalized curves are presented, with the actual normalization constants shown in the tables on the graphs. The quantity Φ_n has been so defined that it is identically zero when

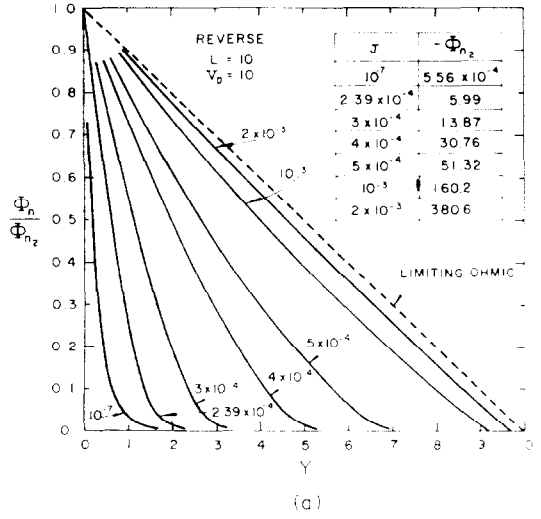

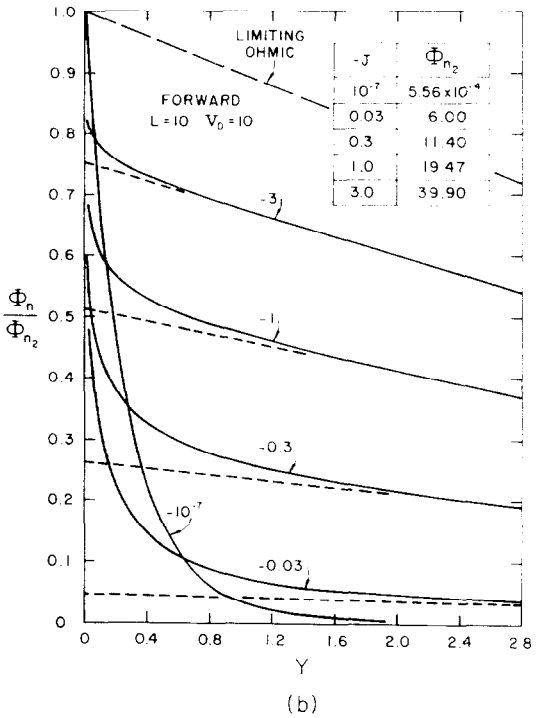

FIG. 9. Dependence of normalized quasi-Fermi-level potential on distance for various current values (junction at left).

$J = 0$. Therefore curves for $J = \pm 10^{-7}$ have been included which indicate the shape to be expected

in the limit of low currents. The two parts of Fig. 9 show the two quite different ways the Φ_n curve approaches a linear distance dependence as the current increases in either the reverse or the forward direction.

When space charge is either absent or independent of position between electrodes, the material behaves ohmically and therefore exhibits a linear current–voltage relation. When Φ_n depends linearly on X as it does for the limiting ohmic lines in Fig. 9, equation (11) shows that $\eta(X)$ is constant and that the charge distribution thus does not vary with position. For $\eta(X)$ to be constant requires either that Φ_n and Ψ be constant or that they vary identically with distance. In the present instance Ψ will thus also depend linearly on distance, and the electric field in the material will be constant, as expected for ohmic behavior. For the limiting ohmic line in Fig. 9(a), Ψ will be given by $(\Phi_n - V_D)$ between the electrodes (except immediately at the ohmic electrode), while in Fig. 9(b) the Ψ corresponding to the ohmic line will be given by $\Psi = \Phi_n$ (except immediately at the barrier electrode).

If V_D is specified and fixed at the barrier contact, the largest difference between Ψ and Φ_n anywhere in the material cannot exceed $|V_D|$ for any current level. However, when the maximum value of $|\Phi_n|$ is of the order of or less than V_D, the shapes of $\Phi_n(X)$ and $\Psi(X)$ curves can differ appreciably. On the other hand, when $|\Phi_n|$ greatly exceeds $|V_D|$ over most of the region between electrodes, the $|\Phi_n|$ and $|\Psi|$ curves will be almost the same over this region.

Finally, the distance dependence of various quantities is of interest when both contacts to the specimen are non-ohmic. Results obtained for $L = 10$ and with $V_D = 10$ at both ends are shown in Fig. 10. For comparison with zero-current results,[11] the anode is at the left and the cathode is the right; thus, the contact at the left is forward biased, that at the right reverse biased. In calculating these curves with the computer, integration was usually carried out from left to right starting with an initial value of E, $\Psi = -10$, and $\Phi_n = 0$. The zero of quasi-Fermi-level potential is thus taken, as shown in Fig. 10(a), so that the anode is at ground and the total applied voltage, Φ_{n_2}, appears at the cathode.

In the small-current limit, the curves of Fig. 10(a) become antisymmetric about the center line between the electrodes. Even in the zero-current case, Fig. 10(b) shows that there is a small amount of space charge at the center because of the finite

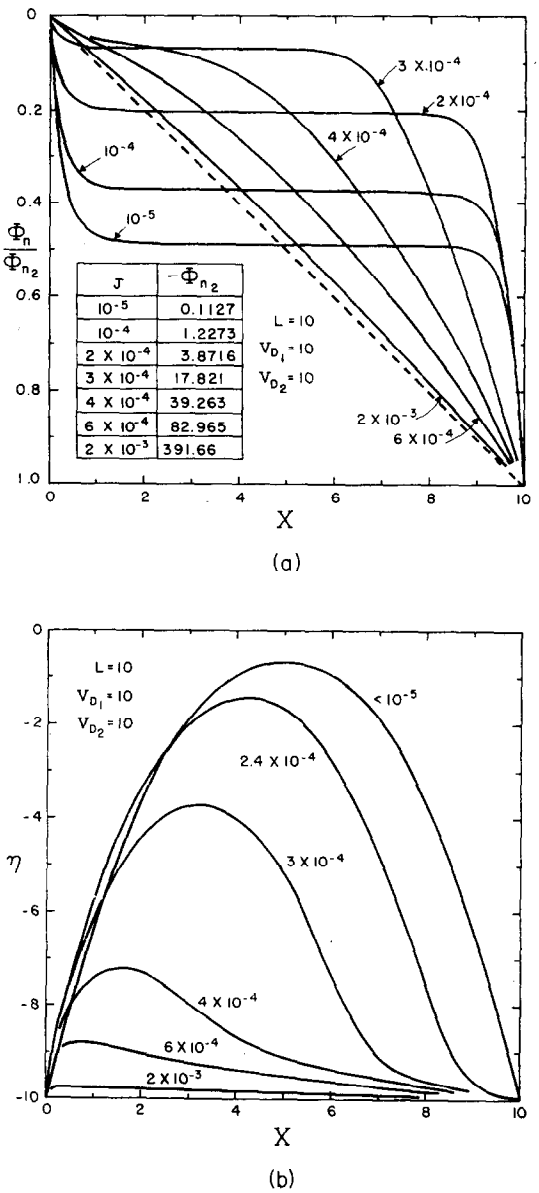

FIG. 10. Distance dependence of Φ_n/Φ_{n_2} and η for various current values for two identical barrier junctions (forward-biased junction on left, reverse-biased on right).

length considered. The curves of Fig. 10 are made up of both forward- and reverse-biased barrier parts and show clearly the dominating effect of the reverse-biased junction region on the over-all combination as the current increases. Only at the lowest currents shown in Fig. 10 does the electric field deviate appreciably from linear distance dependence.

The present $\Phi_n(X)$ curves are surprisingly similar, but not identical, in shape to $\Psi(X)$ curves previously calculated for the zero-current case.[11] In addition to the distinction between non-zero and zero current conditions, the present results apply only to the case where there is an exhaustion-type barrier at each electrode while the earlier $\Psi(X)$ curves apply only when there is exhaustion at one electrode and accumulation at the other. Therefore, the curves are not really comparable, and it is a coincidence that the shapes are so similar.

Most writers who have used the potential-probe method of investigating space-charge distributions have implicitly or explicitly assumed that the probe measures the electrostatic potential at the point probed.* In a one-carrier, one-dimensional system, a potential probe will actually measure the quasi-Fermi-level potential of the mobile carriers, however, provided the electron temperature remains very close to that of the lattice, and in certain regions this quantity can differ by an amount as large as V_D from the electrostatic potential. The situation is appreciably more complicated when charges of both signs are mobile, and separate quasi-Fermi-levels must be introduced for each. These quantities are not equal except under ohmic conditions or at the electrodes, but the application of a metallic potential probe will force their equality at the point of application. Such forced equality will slightly perturb the charge and field distributions within the material even when the probe draws no current, and will thus destroy the one-dimensional character of the current flow.

The $\Phi_n(X)$ curves of Figs. 9 and 10 show the potential distributions which could actually be measured by a potential probe in the non-zero-current case. In the earlier work of the author,[10,11] it was correctly stated that potential probes could not be used to determine the electrostatic potential distribution present in the material in the absence of a potential difference externally applied to the electrodes, but it was implied that probes could measure the electrostatic potential at a point in the material even in the zero-current case in the presence of an externally applied potential. This conclusion is wrong, and the comparison made[11] between the earlier calculated $\Psi(X)$ curves and the experimental potential distributions obtained with potential probes by JOFFE[53] is entirely vitiated.

It is not entirely clear from JOFFE's work whether the current observed in quartz and calcite crystals was primarily of a single charge type or not. If so and if recombination was negligible, his curves are comparable with those of Fig. 10(a). It should be noted, however, that although his curves are of the general shape of those of Fig. 10(a), he was concerned with potential differences of the order of 100 V, while the largest Φ_{n_2} in Fig. 10(a) corresponds to about 10 V at room temperature. It is probable that larger values of L and V_D than here used could be selected which would make theoretical curves such as those of Fig. 10(a) approximate to those of JOFFE in magnitude as well as in shape.

When the potential-probe method of measuring quasi-Fermi-level potential distributions within a material is not pertinent or practical, other methods of investigating the distance dependence of various quantities of interest must be used. CROITORU[54] has shown that the Kerr effect can be employed to give $\mathscr{E}(x)$ for transparent dielectric liquids. HARRICK[55] has used infrared absorption to probe the distribution of free carriers in semiconductors, and preliminary results of BËR[56] indicate that the field distribution in high-field regions may possibly be directly obtainable from measurement of light absorption at the edge of the fundamental absorption band of the material.

Current–voltage dependence

The current which flows when an external potential difference is applied to the material is determined by the charge conditions throughout the system. Although near the barrier the charge and field distributions may differ appreciably from those predicted by the SCHOTTKY or SPENKE

* A number of references to measurements of this kind are given in Refs. 10 and 11.

solutions, the current is an averaged response, and the exact current–voltage relation may be expected to differ less radically from those predicted by the above theories. Since the SCHOTTKY–SPENKE theories deal only with the barrier region and therefore exclude any ohmic potential drop, the present results, which are calculated for a fixed length and include an ohmic contribution, must be modified to eliminate any ohmic drop, in order to allow direct comparison.

The ohmic potential drop is readily found to be and is compared with the simplest exponential characteristic, that for an ideal rectifier. The constant in the latter has been selected to yield the same limiting low voltage characteristic as that found in the exact solution. For strong revers ebias, the length of the exhaustion region may exceed $L = 10$. Since we are here dealing with the barrier region alone, the actual length used in calculating the reverse characteristic has been purposely taken appreciably greater than E_2 so that it is always considerably greater than the

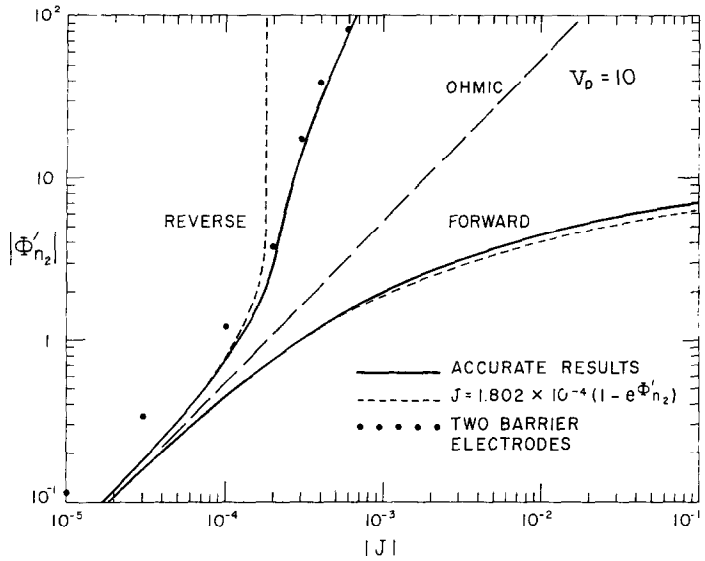

FIG. 11. Log–log current–voltage relations for barrier region alone (except for solid dots which pertain to a fixed length $L = 10$ and two barrier electrodes).

$-JL$; therefore, the new potential variable $\Phi'_{n_2} \equiv \Phi_{n_2} + JL$ may be used for comparisons restricted to the barrier region alone. It is the applied potential drop across only the barrier region in the SCHOTTKY–SPENKE theories. In the present work, where the approximation of an explicit barrier thickness is not made, Φ'_{n_2} is simply the total applied potential difference less the ohmic drop occurring in the total length L. There is no significant difference between Φ_{n_2} and Φ'_{n_2} for the range of reverse currents and lengths considered herein; it is only in the forward direction that appreciable difference appears.

In Fig. 11 the exact current–voltage dependence for the barrier region is shown on a log–log plot

effective exhaustion length. The limiting current–voltage relation is then approximately

$$J = [2V_D - \Phi'_{n_2})]^{1/2} \exp(-V_D),$$

and $|J|$ thus eventually becomes proportional to $|\Phi'_{n_2}|^{1/2}$. On the other hand, when L is fixed, the exhaustion region soon fills almost the entire region, as in the $J = 2 \times 10^{-3}$ curve of Fig. 8. As the applied potential is further increased in this region, it is found that $|J|$ becomes proportional to $|\Phi_{n_2}|$. Such ohmic behavior follows because the charge distribution, which is exhausted down to the level $N = \exp(-V_D)$, cannot change appreciably with current after this condition is reached. It turns out that there is little difference

between the field E_2 at the reverse-biased junction for the case when the length of the sample is appreciably greater than the exhaustion region and that when the length is fixed and less than the exhaustion region would be for a given reverse potential difference in the first case. On the other hand, the field E_1 at the ohmic contact is quite different in the two cases, being very small in the first and approaching (E_2-L) in the second.

The present curves can easily be used to construct the current–voltage characteristic for two identical junctions in series, such as would be obtained if the separation between barrier regions were always sufficient that a region of essentially zero space charge appeared between the electrodes for all applied biases. For a given applied voltage, one junction would be forward biased and the other reverse biased. The total potential difference would then be made up, for a given current, of the forward barrier drop plus the reverse drop plus any ohmic potential drop.

The situation is somewhat different when the length is fixed and small enough that most of the material between electrodes becomes appreciably exhausted when an external potential difference is applied. The results for such a case are illustrated by the large solid dots in Fig. 11. Here, two identical electrodes each with $V_D = 10$ were considered for a fixed length $L = 10$. For high applied bias, the influence of the forward-biased junction is negligible and the over-all response approaches that of a single reverse-biased junction. Since the material becomes exhausted down to the $N = \exp(-V_D)$ level, the final limiting characteristic for this case will involve direct proportionality between $|J|$ and $|\Phi_{n_2}|$. In the limit of low applied potentials, conditions at the two junctions are identical, however, and the zero-current resistance is thus twice that of a single junction. It is worth mentioning that for $|\Phi'_{n_2}| \ll 1$, where the current–voltage relation is linear and hence ohmic, there is still space charge in the neighborhood of barrier contacts, as shown for example in Fig. 9. Such ohmic behavior is found whenever the space-charge distribution is zero or independent of current.

Fig. 12 is a linear plot of the forward characteristic for various conditions. The two heavy solid lines show the exact results for $L = 5$ and 10. The dashed lines are the asymptotes which the exact solutions approach as $|J|$ increases. Note that they may be used to determine V_D. When Φ_{n_2} is modified by subtraction of the ohmic drop, it is

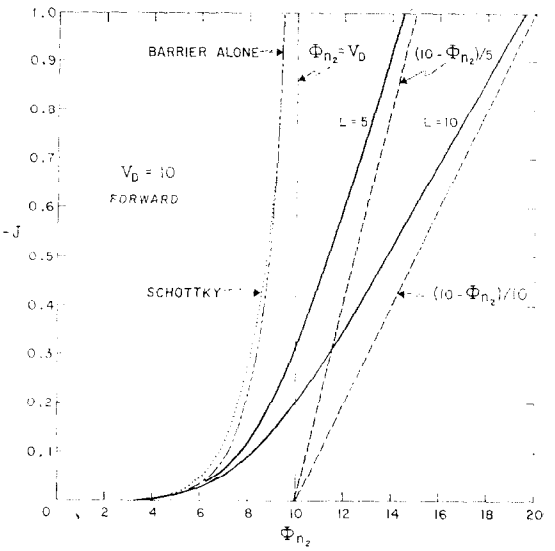

FIG. 12. Linear plot of current–voltage relations in the forward direction showing corrections for ohmic drops.

found that the resulting characteristic for the barrier alone is independent of length, as it should be. Thus both the $L = 5$ and $L = 10$ curves lead to the same barrier characteristic. Over part of the range, the predictions of the simple SCHOTTKY theory are also shown for comparison.

Finally, Fig. 13 shows the forward characteristic on a semi-log basis. The dashed line shown at the extremes of the heavy exact barrier characteristic denotes the best straight-line approximation to this characteristic. It is clear that over about three decades of current an exponential approximation to the exact solution is quite adequate. Instead of involving $\exp(\Phi'_{n_2})$, however, the straight line shown implies $\exp(\Phi'_{n_2}/1{\cdot}15)$. The number 1·15 will, of course, be a function of V_D.

Table 2 presents a comparison between the predictions of various current–voltage characteristics for the barrier region alone. Here J_e is the exact current. The SCHOTTKY formula used was[51]

$$J_{sc} = \frac{\sqrt{(-2\Psi_2)}\exp(-V_D)[1-\exp(\Phi'_{n_2})]}{[1-\exp(2\Psi_2)]} \tag{27}$$

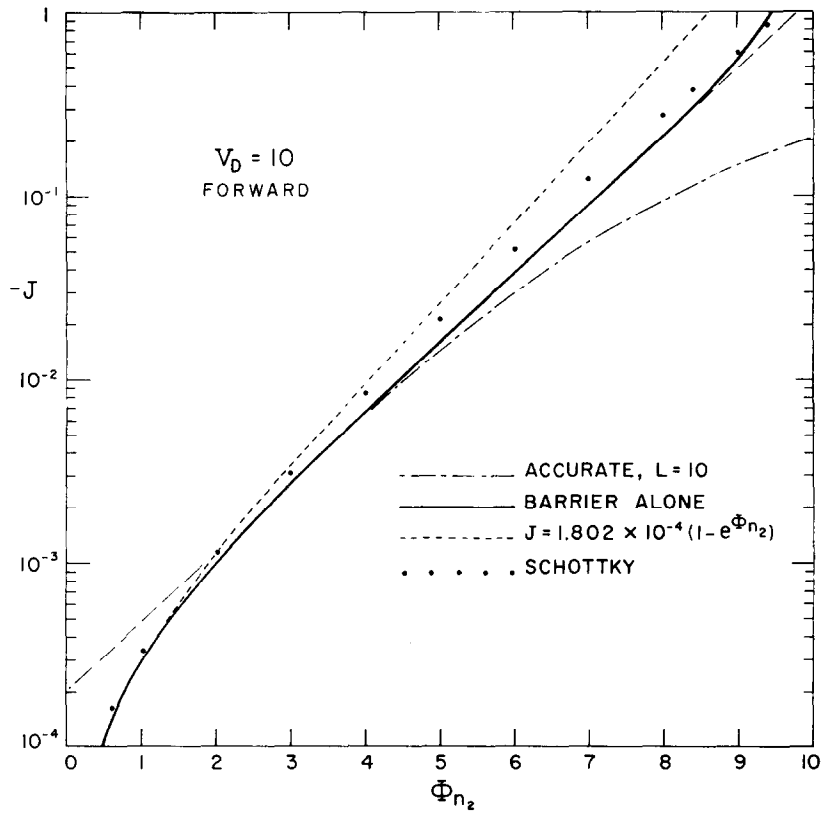

FIG. 13. Log-linear forward current–voltage characteristics.

where Ψ_2 is given here and below by $(\Phi'_{n_2} - V_D)$. The modified SCHOTTKY formula employed was

$$J_{msc} = \frac{E_2 \exp(-V_D)[1 - \exp(\Phi'_{n_2})]}{[1 - \exp(-E_2^2)]} \tag{28}$$

where

$$E_2 = [2\{-\Psi_2 - 1 + \exp(-V_D)\}]^{1/2} \tag{29}$$

This approximate expression for E_2 was used only when $-\Psi_2 > 1$. Finally, SPENKE's result may be expressed as

$$J_{sp} = \frac{\exp(-V_D)[1 - \exp(\Phi'_{n_2})]}{\sqrt{(2)}\exp(\Psi_2)\,\mathrm{erfi}\sqrt{(-\Psi_2)}} \tag{30}$$

where erfi(ξ) has already been defined.

The results of Table 2 show that in the reverse direction all three expressions are adequate, but the J_{sp} and J_{msc} forms are clearly superior to the J_{sc}. Since the expression for J_{msc} is considerably simpler than that for J_{sp} and yet yields almost as accurate results, the former will usually be preferred. As the current increases in the forward direction, the accuracy of the three expressions decreases for an appreciable range, then increases, and finally decreases. As might be expected, none of the solutions is adequate in the high-forward-current range. This is not usually of importance since, even if the present exact solution applied closely to experimental results in the high forward range, the barrier-region characteristic would be masked by ohmic potential drops associated with the fixed and finite length of the sample.

Fig. 14 compares the accurate dependence of E_2^2 on Φ'_{n_2} with the linear predictions of the SCHOTTKY theory. The dotted barrier-region curve and the SCHOTTKY line are, of course, plotted vs. Φ'_{n_2}. At about $\Phi'_{n_2} = 9{\cdot}3$, E_2 passes through zero and

Table 2. Comparison of various current productions (barrier layer alone; $V_D = 10$)

$\lvert J_e \rvert$	Forward			Reverse		
	J_{sc}/J_e	J_{msc}/J_e	J_{sp}/J_e	J_{sc}/J_e	J_{msc}/J_e	J_{sp}/J_e
0	1·127	1·069	1·062	1·127	1·069	1·062
10^{-5}	1·128	1·069	1·062	1·126	1·068	1·062
2×10^{-5}	—	—	—	1·125	1·068	1·062
3×10^{-5}	1·129	1·070	1·063	—	—	—
4×10^{-5}	—	—	—	1·123	1·067	1·060
10^{-4}	1·134	1·073	1·066	1·115	1·062	1·057
2×10^{-4}	—	—	—	1·092	1·049	1·046
$2·5\times10^{-4}$	—	—	—	1·066	1·034	1·033
3×10^{-4}	1·146	1·080	1·071	1·046	1·024	1·023
4×10^{-4}	—	—	—	1·026	1·013	1·012
6×10^{-4}	—	—	—	1·011	1·006	1·006
10^{-3}	1·169	1·094	1·081	1·004	1·002	1·002
2×10^{-3}	—	—	—	—	—	—
3×10^{-3}	1·204	1·113	1·094	—	—	—
10^{-2}	1·260	1·141	1·109	—	—	—
3×10^{-2}	1·324	1·161	1·113	—	—	—
10^{-1}	1·364	1·124	1·073	—	—	—
3×10^{-1}	1·252	1·051	0·964	—	—	—
6×10^{-1}	1·073	—	0·871	—	—	—
8×10^{-1}	0·990	—	0·833	—	—	—
1	0·930	—	0·807	—	—	—
1·4	0·853	—	0·773	—	—	—
3	0·750	—	0·727	—	—	—

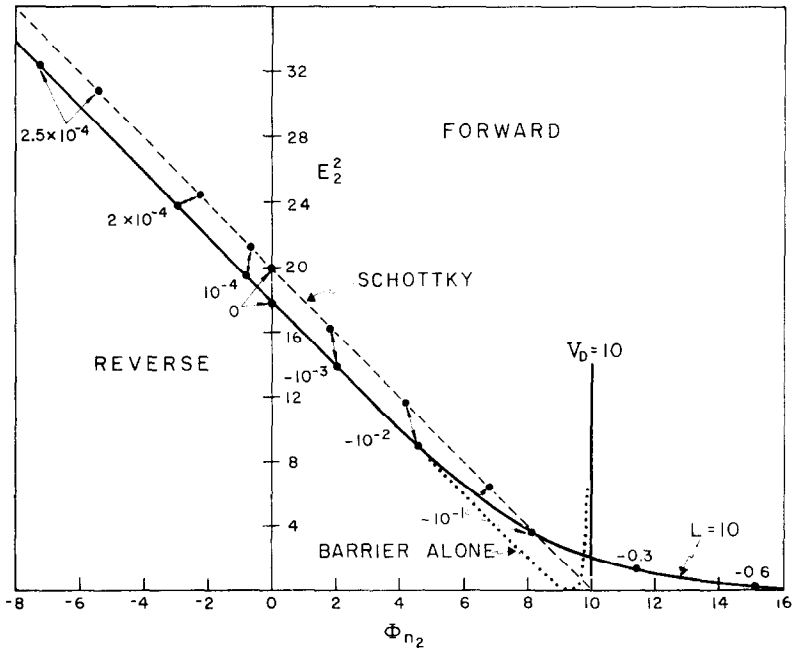

FIG. 14. E_2^2 vs. Φ_{n_2} showing comparison with SCHOTTKY-theory predictions and dependence of accurate E_2^2 on barrier-region potential drop as well.

becomes negative. In this high-current region, it and E_1 both approach J. The lines joining the heavy dots in Fig. 14 show where points for a given current fall for the exact and SCHOTTKY lines and thus indicate further deviations between the two calculations.

Resistance

Fig. 15 shows the dependence of (normalized) resistance $\mathscr{R}$ on the total applied voltage Φ_{n_2} across a slab of thickness L. This integral or static

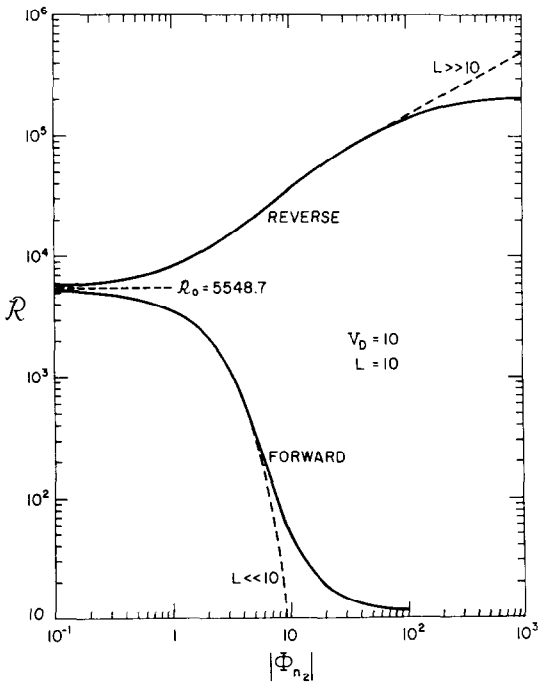

FIG. 15. Dependence of junction static resistance on total applied potential difference.

resistance is simply $-\Phi_{n_2}/J$. The normalizing resistance is thus $kTL_D/e^2D_n n_\infty$. The curves for the differential resistance, $-d\Phi_{n_2}/dJ$, are quite similar in appearance to those for the integral resistance. When L is always taken appreciably greater than E_2 and the length of the exhaustion region, the $\mathscr{R}$ for the barrier alone will become proportional to $|\Phi'_{n_2}|^{1/2}$ for strong reverse bias, in agreement with the discussion of Fig. 11. When the length is fixed, $\mathscr{R}$ will approach constancy and ohmic behavior for both high-reverse and high-forward bias. Sooner or later, deviations from the reverse-bias behavior shown in Fig. 15 must occur because of high-field breakdown in the material. The final limiting $\mathscr{R}$ in the forward direction is just L, since J then approaches $-\Phi_{n_2}/L$. The dashed line in the forward direction marked $L \ll 10$ shows the resistance for the barrier region alone.

The zero-current resistance $\mathscr{R}_0$ of the junction is a quantity of some interest. It can be calculated directly for the cases defined by equations (27–30), but must be obtained by interpolation from the accurate computer solutions for several very low currents. The results for $V_D = 10$ are 5548·7, 5224·6, 5191·7 and 4925·3 for the computer, SPENKE, modified SCHOTTKY and SCHOTTKY solutions, respectively. The SCHOTTKY value of $\mathscr{R}_0$ is $2 \sinh V_D/\sqrt{2V_D}$. When the true zero-current field $E_2 \cong (2(V_D-1))^{1/2}$ is used in the SPENKE solution instead of the SCHOTTKY field $E_2 = (2V_D)^{1/2}$, the resulting $\mathscr{R}_0$ is very close to the accurate value for $V_D \geqslant 10$.

Capacitance

In Fig. 16(a) the accurate and SCHOTTKY results for the normalized differential capacitance are compared for $V_D = 10$. Although the accurate curves are plotted from the computer evaluation of equation (21), this equation itself is somewhat approximate, as mentioned earlier. The SCHOTTKY curves apply for the barrier region alone and yield a capacitance which indefinitely increases in the forward direction and decreases toward zero in the reverse direction. The main difference between the accurate and SCHOTTKY curves in the low-bias region arises from the presence of the (V_D-1) term in the accurate expression for E_2 as compared to V_D alone in the SCHOTTKY expression for this quantity.

For larger bias, the accurate and SCHOTTKY curves deviate in addition because the computer results apply to the entire slab, not just the barrier region. Thus, the accurate results include the effect of the geometrical capacitance of the material as well and, in the high-forward-bias or reverse-bias limits, the capacitance approaches the geometrical value and $(C_d/C_0) \to L^{-1}$. The computer results therefore are directly comparable to the results of capacitance measurements on a material of fixed length having one ohmic and one barrier electrode.

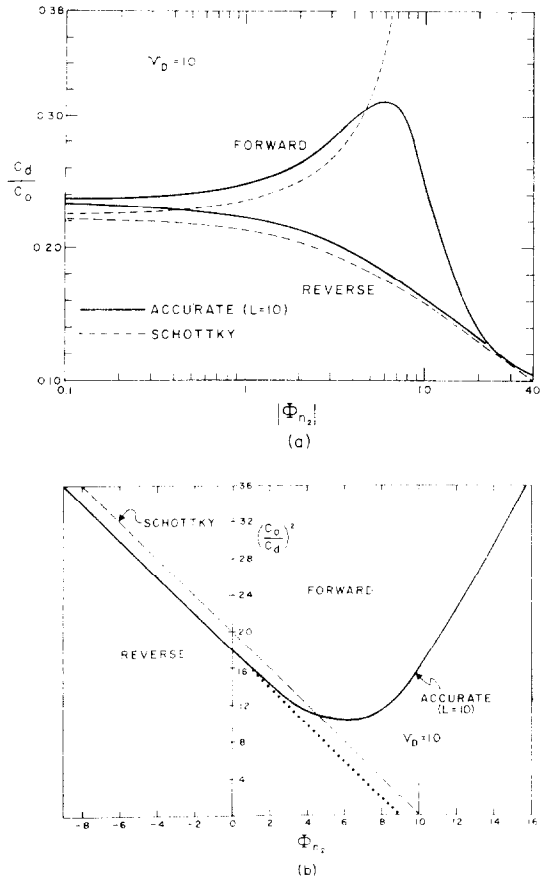

FIG. 16. Normalized differential capacitance and $[C_0/C_d]^2$ vs. applied potential difference with comparison to SCHOTTKY-theory predictions.

Because the field is in general non-uniform through the entire length between contacts, the space-charge and geometrical capacitances of the material cannot be considered to be in either series or parallel. Further, as long as the field is non-uniform the geometrical capacitance, insofar as it can be defined, is not even equal to the constant limiting value of equation (24). However, in the limit of high bias and ohmic behavior, the field is essentially uniform and the geometrical capacitance is all that is of importance and has its usual value. The above considerations make it not worthwhile to try to combine the geometrical capacitance with the SCHOTTKY space-charge capacitance to obtain over-all capacitances which could be directly compared with the accurate results for the whole slab.

Fig. 16(b) shows the capacitance plotted in the conventional inverse-square manner. This graph should be compared with that of Fig. 14 for E_2^2. In the reverse direction, equation (23) shows that $(C_0/C_d)^2$ is closely equal to E_2^2. Thus, a comparison of Figs. 14 and 16(b) shows clearly the region where the above near equality begins to fail badly. The deviation of C_d^{-2} from a straight line has been ascribed by SHIVE[57] to either a bias-dependent V_D or to non-uniform doping of the material. It is evident from Fig. 16(b) that deviation can occur even in the absence of both of these effects. Because of the difficulty of measuring capacitance accurately in the low-resistance, appreciable forward bias region, no measurements showing an actual increase in $(C_0/C_d)^2$ like that in Fig. 16(b) seem available, although many measurements show deviations in the right direction from straight-line behavior. Note that for $L \gg 1$ the higher V_D the wider the range over which a straight-line dependence will be found.

Fig. 16(b) shows that the intercept of the straight-line extrapolation of the C_d^{-2} curve with the Φ_{n_2} axis is the WAGNER value $(V_D - 1)$ while the SCHOTTKY intercept is V_D. When experimental C_d^{-2} plots have been analyzed, it has been almost invariably assumed that the intercept yielded V_D. This error is self-compensating and leads to no error in N_D if the latter is calculated from the SCHOTTKY capacitance formula as well. Further, the actual difference between V_D and $(V_D - 1)$ will usually be quite small for most experimental V_D's at room temperature and below. On the other hand, wherever $\exp(-V_D)$ occurs, as in expressions for the current and resistance, the assumption that $(V_D - 1)$ is actually V_D leads to an error of a factor of e^1. If N_D has been determined correctly from capacitance measurements, the dielectric constant is assumed known and the mobility μ_n is to be determined from current–voltage results, the unwitting use of $(V_D - 1)$ in place of V_D can lead to an apparent mobility e^{-1} times the true mobility, even aside from other smaller errors incident to using an approximate equation such as (27), (28) or (30) instead of more accurate results.

Finally, it may be mentioned that when both

electrodes are partly blocking, the space-charge capacitances localized near each electrode can be added in series to obtain the over-all capacitance, provided the separation between electrodes is sufficiently great that there is a region of essentially zero space charge between the two barrier regions. This matter has been considered at some length for the zero-current case in earlier work.[11] Again, the final limiting capacitance is the geometrical value. The results for two identical partly or completely blocking electrodes can also be applied to the case of back-to-back barrier contacts such as that considered in SiC by STRATTON[58]. It is only necessary that the length of material between outside ohmic contacts in the back-to-back case equal the length between barrier electrodes in the two-barrier case and that this length be great enough for essentially ohmic, zero-space-charge conditions to exist at the center. In both cases there will be one forward- and one reverse-biased junction and the over-all behavior will be the same.

Acknowledgements—The author is greatly indebted to Dr. ROBERT STRATTON and to Professor P. T. LANDSBERG for many valuable discussions and comments.

REFERENCES

1. G. GOUY, *J. Phys. Radium* **9,** 457 (1910).
2. D. L. CHAPMAN, *Phil. Mag.* **25,** 475 (1913).
3. R. H. FOWLER, *Statistical Mechanics* (1st Ed.) pp. 282–283. Cambridge University Press, London (1929).
4. H. MÜLLER, *Cold Spr. Harb. Symp. Quant. Biol.* **1,** 1 (1933).
5. J. R. MACDONALD and M. K. BRACHMAN, *J. Chem. Phys.* **22,** 1314 (1954).
6. L. GOLD, *J. Electron Control* **5,** 427 (1958).
7. D. C. GRAHAME, *Chem. Rev.* **41,** 441 (1947).
8. J. R. MACDONALD, *J. Chem. Phys.* **22,** 1317 (1954).
9. K. BOHNENKAMP and H. J. ENGELL, *Z. Electrochem.* **61,** 1184 (1957).
10. J. R. MACDONALD, *J. Chem. Phys.* **29,** 1346 (1958).
11. J. R. MACDONALD, *J. Chem. Phys.* **30,** 806 (1959).
12. T. M. PROCTOR and P. M. SUTTON, *J. Chem. Phys.*, **30,** 212 (1959).
13. C. WAGNER, *Phys. Z.* **32,** 641 (1931).
14. J. F. DEWALD, *Bell Syst. Tech. J.* **39,** 615 (1960).
15. H. K. HENISCH, *Rectifying Semiconductor Contacts.* Oxford University Press, London (1957).
16. E. SPENKE, *Electronic Semiconductors.* McGraw-Hill, New York (1958).
17. H. K. HENISCH, *Rectifying Semiconductor Contacts* p. 192. Oxford University Press, London (1957).
18. (a) H. Y. FAN, *Phys. Rev.* **74,** 1505 (1948); (b) E. I. ADIROVICH, *Soviet Phys. Solid State* **2,** 1282 (1961); (c) G. T. WRIGHT, *Solid-State Electron.* **2,** 165 (1961).
19. (a) W. SHOCKLEY and R. C. PRIM, *Phys. Rev.* **90,** 753 (1953); (b) P. T. LANDSBERG, *Z. phys. Chem.* **198,** 75 (1951).
20. G. C. DACEY, *Phys. Rev.* **90,** 759 (1953).
21. S. M. SKINNER, *J. Appl. Phys.* **26,** 498 (1955).
22. S. M. SKINNER, *J. Appl. Phys.* **26,** 509 (1955).
23. G. H. SUITS, *J. Appl. Phys.* **28,** 454 (1957).
24. M. A. LAMPERT, *Phys. Rev.* **103,** 1648 (1956).
25. M. A. LAMPERT, *J. Appl. Phys.* **29,** 1082 (1958).
26. R. H. PARMENTER and W. RUPPEL, *J. Appl. Phys.* **30,** 1548 (1959).
27. M. A. LAMPERT, *R.C.A. Rev.* **20,** 682 (1959).
28. M. A. LAMPERT, *Phys. Rev.* **121,** 26 (1961).
29. D. O. VAN OSTENBURG and D. J. MONTGOMERY, *Text. Res. (J.)* **28,** 22 (1958).
30. R. SEIWATZ and M. GREEN, *J. Appl. Phys.* **29,** 1034 (1958).
31. J. L. MOLL, *Proc. I.R.E.* **46,** 1076 (1958).
32. P. WINKEL and B. VERKERK, *Philips Res. Rep.* **13,** 501 (1958).
33. N. F. MOTT, *Proc. Roy. Soc.* **A171,** 27, 144 (1939).
34. W. SCHOTTKY, *Naturwissenschaften* **26,** 843(193 8); *Z. Phys.* **113,** 367 (1939); **118,** 539 (1942).
35. W. SCHOTTKY and E. SPENKE, *Wiss. Veröff. Siemens* **18,** 225 (1939).
36. E. SPENKE, *Z. Phys.* **126,** 67 (1949); *Z. Naturf.* **4a,** 37 (1949).
37. P. T. LANDSBERG, *Proc. Roy. Soc.* **A206,** 463 (1951).
38. P. T. LANDSBERG, *Proc. Phys. Soc. Lond.* **B68,** 366 (1955).
39. P. T. LANDSBERG, *Proc. Roy. Soc.* **A206,** 477 (1951).
40. J. N. SHIVE, *Semiconductor Devices* p. 375. Van Nostrand, Princeton (1959).
41. T. NUMATA, *J. Phys. Soc. Japan* **14,** 902 (1959).
42. D. N. NASLEDOV and I. M. YASHUKOVA, *Soviet Phys. Solid State* **1,** 1087 (1960).
43. E. SPENKE, *Electronic Semiconductors,* p. 307 ff. McGraw-Hill, New York (1958).
44. P. T. LANDSBERG, *Proc. Roy. Soc.* **A213,** 226 (1952).
45. R. STRATTON, Private communication.
46. E. SPENKE, *Electronic Semiconductors* pp. 46, 317. McGraw-Hill, New York (1958).
47. E. SPENKE, *Electronic Semiconductors* pp. 309, 318. McGraw-Hill, New York (1958).
48. W. SHOCKLEY, *Bell Syst. Tech. J.* **28,** 435 (1949).
49. E. SPENKE, *Electronic Semiconductors,* pp. 356–363. McGraw-Hill, New York (1958).
50. R. STRATTON, Private communication. Submitted to *Phys. Rev.*
51. H. K. HENISCH, *Rectifying Semiconductor Contacts,* p. 207. Oxford University Press, London (1957).
52. J. R. MACDONALD, *Phys. Rev.* **92,** 4 (1953).
53. A. F. JOFFE, *The Physics of Crystals.* McGraw-Hill, New York (1928).
54. Z. CROITORU, *Bull. Soc. Elect.* **1,** 362 (1960).
55. N. J. HARRICK, *Phys. Rev.* **103,** 1173 (1956); *J. Appl. Phys.* **29,** 764 (1958); *J. Phys. Chem. Solids* **14,** 60 (1960).

56. K. V. Bër, *Izv. Akad. Nauk. SSSR, Ser. fiz.* **24,** 36 (1960).
57. J. N. Shive, *Semiconductor Devices* p. 98. Van Nostrand, Princeton (1959).
58. R. Stratton, *Proc. Phys. Soc. Lond.* **B69,** 513 (1956).

APPENDIX I

Non-Zero Recombination

Let N_D^n be the local concentration of neutral donors. Then at any point in the material we must have $N_D \equiv N_D^n + N_D^+$. In addition, in equilibrium we may write

$$\frac{\partial N_D^n}{\partial t} = -k_1 N_D^n + k_2 n N_D^+ = 0 \qquad \text{(A.1)}$$

where k_1 is a dissociation rate constant and k_2 a recombination rate constant.[52] We may now define the new recombination constant $R \equiv k_2 N_D / k_1$. Equation (A.1) then leads to the mass-action result[46]

$$\left(1 - \frac{N_D^+}{N_D}\right) = R\left(\frac{N_D^+}{N_D}\right)\left(\frac{n}{N_D}\right) \qquad \text{(A.2)}$$

where N^+ and n may be functions of position. This equation holds only when the Maxwell–Boltzmann approximation, equation (5), is applicable. In the non-zero-recombination case, $R \neq 0$, and n and N_D^+ have the common value n_∞ ($\neq N_D$) in space-charge-free bulk material. Then (A.2) becomes

$$\left(1 - \frac{n_\infty}{N_D}\right) = R\left(\frac{n_\infty}{N_D}\right)^2 \equiv r \qquad \text{(A.3)}$$

where a new recombination constant r $(0 \leqslant r \leqslant 1)$ has been introduced. Equation [A.3] leads to

$$\frac{n_\infty}{N_D} = 1 - r = -\frac{1}{2R} + \left[\left(\frac{1}{2R}\right)^2 + \frac{1}{R}\right]^{1/2} \qquad \text{(A.4)}$$

which shows how R or r determines the mobile charge concentration in space-charge-free bulk material. On normalizing with n_∞, (A.2) becomes

$$\begin{aligned}\frac{N_D^+}{n_\infty} &= \left(\frac{N_D}{n_\infty}\right)\left[1 - R\left(\frac{n_\infty}{N_D}\right)^2\left(\frac{N_D^+}{n_\infty}\right)\left(\frac{n}{n_\infty}\right)\right] \\ &= (1-r)^{-1}[1 - rN(N_D^+/n_\infty)] \\ &= [1 + r(N-1)]^{-1} \qquad \text{(A.5)}\end{aligned}$$

Since $N \equiv n/n_\infty$ is still given by (8) in the present case, (A.5) may be introduced into (2) to yield the appropriate Poisson equation when $R \neq 0$. Let the Debye length L_D used in the body of the paper for normalization be replaced everywhere by the effective Debye length[10,11] $L_e \equiv \theta L_D$, where

$$\theta = [(1+r)(1-r)]^{-1/2}.$$

Then the form of equations (9) and (11) remains the same and (10) becomes

$$\begin{aligned}\frac{dE}{dX} &= (1+r)^{-1}\left[\frac{1}{1+r(N-1)} - N\right] \\ &= [1-N]\left\{\frac{(1+r)^{-1}(1+rN)}{1+r(N-1)}\right\}\end{aligned} \qquad \text{(A.6)}$$

where the term in curly brackets represents the correction for non-zero recombination. Equation (A.6) has been termed a Poisson–Boltzmann equation by Dewald[14], but such nomenclature is misleading since the donors obey Fermi not Maxwell–Boltzmann statistics here.

Finally, it is of interest to express R and r in terms of the energy levels of the semiconductor. The usual expression for N_D^+ is[47]

$$N_D^+ = N_D\{1 + 2\exp[(E_F - E_D)/kT]\}^{-1} \qquad \text{(A.7)}$$

where the factor of 2 in (A.7) arises from the spin degeneracy of the donor state. On substituting (5) and (A.7) into (A.2), one obtains

$$\begin{aligned}R &= \frac{2N_D}{N_C}\exp[(E_C - E_D)/kT] \\ &\equiv \frac{2N_D}{N_C}\exp(E_{CD}/kT)\end{aligned} \qquad \text{(A.8)}$$

where the energy difference E_{CD} is constant throughout the material for both equilibrium and non-equilibrium conditions. The quantity r can be expressed in a number of ways. One of the most interesting is obtained using (A.7) in (A.3) and noting that $n_\infty \equiv N_{D_\infty}^+$; then

$$r = 1 - (N_{D_\infty}^+/N_D) = \{[1 + \tfrac{1}{2}\exp[(E_{D_\infty} - E_{F_\infty})/kT]\}^{-1} \qquad \text{(A.9)}$$

Thus, r is just the probability with which a donor level is occupied by an electron, in agreement with the relation $N_{D_\infty}^n = rN_D$. The recombination coefficients R and r depend on radiation as well as temperature provided absorbed quanta are of sufficient energy to ionize neutral donors.

APPENDIX II

Computation Details

An IBM 650 computer has been used to solve the three differential equations, (9–11), simultaneously by a step-by-step, fourth-order Runge–Kutta procedure. In such calculations the current J must be specified and

the resulting applied voltage determined at the completion of the solution. When the length between electrodes is specified, as is usually the case here, one must begin the calculation with specified values of E, Φ_n and Ψ and continue computation until the desired length has been reached, where it is hoped that specified boundary conditions will also be met. In this case, we must solve a two-point boundary-value, or "jury", problem. For example, we shall usually integrate from the ohmic to the barrier contact. Then we can take $\Phi_{n_1} = \Psi_1 = 0$, and we must choose E_1 such that the condition $-\eta_2 = V_D$ is met when X has progressed to the desired L-value. Exact determination of E_1 will therefore require successive approximations. When integration is commenced from the barrier electrode, it is necessary that E_2, Φ_{n_2} and Ψ_2 be known at the beginning of the calculation for given J and L. Such knowledge is usually unavailable until the problem has been run through first the opposite way from ohmic to barrier contact. Once this has been done, the results may be used for a calculation running from $X = L$ to $X = 0$. Such an integration is valuable as a check of the accuracy of the computations since it should finally yield $\Phi_{n_1} = \Psi_1 = 0$ and the original value of E_1 when X reaches zero.

Although the E_1 value which results in satisfaction of the desired boundary conditions at $X = L$ for given choice of J and L can often be estimated quite closely, the attainment of accurate results usually requires that several values of E_1 be tried until one is found for which the boundary conditions are sufficiently closely met. We must select E_1 such that both X and $\eta(X)$ are simultaneously close enough to the selected values of L and η_2, respectively, at the end of the integration. In order to help meet this requirement, an iteration routine has been incorporated into the digital computer program which automatically selects those final-length increments which result in $-\eta_2$ exactly equalling a specified value of V_D. The computer run is then concluded. If the resulting final-length value is not close enough to that desired, the run is repeated with a better choice of E_1.

The length L is a function of $\epsilon \equiv E_1 - J$, as already mentioned. For $\epsilon < 1$, it turns out that for a given current the relation $L = a - b \ln \epsilon$ holds very well. The quantities a and b are themselves functions of current, however. In the reverse direction b is unity, while it decreases slowly from this value as the current increases in the forward direction. For $V_D = 10$, $a = 4{\cdot}52$ at $J = 0$. In general, it decreases in the forward direction and rapidly becomes asymptotic to E_2 in the reverse direction. The exponential relation between ϵ and L is very useful in estimating the value of E_1 required to yield a desired L-value for a given J.

Considerable attention has been given to minimizing round-off and truncation errors arising in the step-by-step integration. A first step toward this goal was to use variables whose total variation was as small as possible over the range of integration. The present choice of the essentially logarithmic variables Φ_n and ψ rather than the direct variable N results in far smaller and hence more accurate increments in the dependent variables for a given increment or step size in the independent variable.

Secondly, both round-off and truncation error are controlled and reduced by progressive and automatic adjustment of the size of the X-increment throughout the calculation. Such control is accomplished by comparing at each step estimates of the truncation errors of each dependent variable increment with pre-set upper and lower relative and absolute error bounds. Automatic increment control of this kind allows the interval from $X = 0$ to L to be tranversed with a minimum number of increments of varying size consistent with a fixed, specified, local error from truncation. It is particularly appropriate and desirable in the present problem where, even using logarithmic variables, the increment size often varies by a factor of as much as 10^6 over the range from 0 to L. A typical high-accuracy solution with variable step length requires from 100 to 200 steps for $L = 10$.

The accuracy of a given solution can be assessed in three separate ways. Firstly, the results at any step can be compared with the predictions of equation (14). Secondly, a complete run can be repeated with more- and more-stringent upper error bounds until no significant change in any of the results occurs. Finally, a forward run can be run backwards from $X = L$ to $X = 0$ and corresponding points compared. Except at the extremes of current where the accuracy may be slightly impaired, error analysis such as that above shows that the results reported herein are generally accurate to five or six significant figures. Greater over-all accuracy could have been achieved had it been warranted.